TUNABLE DIODE LASERS AND THEIR APPLICATIONS IN TRACE GAS AND LIQUID DETECTION

By

XIANG ZHU, M.Sc.

A Thesis

Submitted to the School of Graduate Studies

in Partial Fulfilment of the Requirements

for the Degree

Doctor of Philosophy

McMaster University

TUNABLE DIODE LASERS AND THEIR APPLICATIONS

DOCTOR OF PHILOSOPHY (1996) McMASTER UNIVERSITY

(Engineering Physics) Hamilton, Ontario

TITLE: Tunable Diode Lasers and Their Applications in Trace Gas and Liquid Detection

AUTHOR: Xiang Zhu, B.Sc. (Lanzhou University)

M.Sc. (Queen's University at Kingston)

SUPERVISORS: Professor D.T. Cassidy

NUMBER OF PAGES: xv, 97

ABSTRACT

The use of InGaAsP semiconductor lasers as radiation sources in gas and liquid detection is described in this thesis. Single mode operation and tunability were studied in several schemes including diode lasers with a short external cavity (SXC), diode lasers with multiple short external cavities (MSXC), and a grating external cavity (GEC) diode laser. Comparisons of SXC, MSXC and GEC lasers are given in terms of tunability, side mode suppression ratio (SMSR), stability, and ease of construction and operation.

In highly sensitive gas detection, the harmonic content of residual amplitude modulation (RAM) for current modulation of the diode lasers was studied based on the concept that the light intensity rather than the electric field is directly modulated by the injection current. Formulae for RAM and the absorption signals are given for injection current modulation spectroscopy with diode lasers. Water vapour was detected by using InGaAsP SXC and DFB diode lasers, and an electronic subtracter was employed to reduce the detection noise. A sensitivity of $\approx 1.6\times10^{-6}$ in units of equivalent absorbance in an equivalent noise bandwidth of 1.25Hz was obtained.

In liquid detection, InGaAsP laser diodes with multiple short external cavities (MSCX's) were developed to provide a wide spectral coverage, up to 72nm spectral coverage was achieved. Liquid detection by MSXC diode lasers was studied in

(PCR) and partial least squares (PLS). A sensitivity of 0.1% H_2O in D_2O was achieved and the limiting noise source was assessed. Three component mixtures of H_2O, acetone and methanol were studied in terms of regression factors and outlier detection in the PCR and the PLS algorithms.

To achieve even broader tunability by means of external cavity, work on making broad gain peak InGaAsP/InP lasers was initiated.

ACKNOWLEDGEMENTS

I would like to express my gratitude to my supervisor, Dr. Daniel T. Cassidy for his guidance and encouragement. I especially benefited from his diverse insights and interests in every aspect of this work.

I would also like to thank Dr. M. Davies and Dr. S. McAlister of the Institute for Microstructure Sciences, National Research Council, for their kindness and support in the design and processing of the broad gain peak diode lasers. Thanks to Dr. D. Thompson and Dr. B. Robinson for the fabrication of the laser structures, and Dr. Q.C. Zhao for the processing of the ridge waveguide lasers. I am very grateful to G. Leinweber and Dr. D. Bruce for helpful discussions on many technical issues. Thanks also to my fellow graduate students for their friendship and assistance which made the time during this research more enjoyable and memorable.

Finally, I would like to thank my parents for their support during my endeavour.

TABLE OF CONTENTS

LIST OF FIGURES

LIST OF TABLES

ABBREVIATIONS & SYMBOLS

DBR:	distributed Bragg reflector
DFB:	distributed feedback
ENBW:	equivalent noise bandwidth
FM:	frequency modulation
FP:	Fabry-Pérot
GEC:	grating external cavity
MIR:	middle-infrared
MSXC:	multiple short external cavity
NIR:	near-infrared
PCR:	principal component regression
PL:	photoluminescence
PLS:	partial least squares
PZT:	piezoelectric transducer
RAM:	residual amplitude modulation
RMSEP:	root-mean-square error of prediction
SMSR:	side mode suppression ratio
SXC:	short external cavity
TEM:	transmission electron micrography
WDM:	wavelength domain multiplex
WM:	wavelength modulation

c:	light velocity
C:	concentration of gas
E:	amplitude of electric-field
g_c, g_e:	total gain of external cavity
g_d:	total gain of diode laser for electric field
$g(\lambda)$:	gain of laser at wavelength λ
g_0:	gain peak
I:	light intensity
J_n:	nth-order Bessel function
k:	gain width coefficient
l:	pathlength
L_c, L_e:	length of external cavity
L_d:	length of active region

n_d:	refractive index of diode laser
n_g:	effective group index of active region
N:	sample number
r, r_L, r_i	facet reflectivity coefficient
r_{eff}:	effective refractive coefficient
R^2:	correlation coefficient
S:	absorption line strength
T:	transmission coefficient
y_i:	concentrations in test group
$\hat{y}_i$:	predicted concentrations
β:	frequency modulation index
γ, Γ:	half-width of absorption line
$\Delta\alpha$:	variation on the loss
$\Delta\nu$:	separation of laser modes
δ_n:	attenuation of field amplitude
λ:	wavelength
λ_0:	wavelength of gain peak
ν_m:	frequency of laser mode
ω_0:	optical frequency
ω_m:	modulation frequency
ϕ_n:	dispersion of field amplitude
ψ:	phase difference between amplitude modulation and frequency modulation

CHAPTER 1 - INTRODUCTION

1.1 Semiconductor Lasers and Trace Species Detection

Since the first semiconductor diode lasers were demonstrated in 1962 [1], semiconductor lasers have improved steadily with regard to reliability, ease of operation and cost, and have had a great impact on science and technology. The notable examples range from optical telecommunication, laser printers, and CD players to applications in realization of Bose-Einstein condensation [2]. The technology of semiconductor lasers itself is far from mature. There are many related physics to be studied and many novel devices and new applications have been proposed and implemented.

The use of semiconductor diode lasers as radiation sources in the trace species detection has been extensively studied [3][4][5] and regarded to have a great potential in environmental pollution monitoring, industrial process control and biomedical diagnosis [6][7][8][9]. However, the practical implementation of laser diodes is sometimes hindered by drawbacks such as limited spectral coverage, multimode operation, and excess noise. Diode laser based spectrometers so far remain as dedicated instruments in laboratories. One motivation of the work reported in this thesis was to investigate ways to overcome

InGaAsP semiconductor lasers are usually designed and constructed to have fundamental spatial mode, which is critical for coupling light into optical fibres. However they normally operate with several longitudinal modes [10]. Single mode operation is desired in spectroscopy for two reasons. First, a diode laser with side modes can give spurious absorption signals when side modes tune through an absorption line [11]. Second, only low sensitivity can be obtained due to the mode partition noise in multimode lasers.

There are many ways to obtain single mode operation. Distributed feedback (DFB) lasers and distributed Bragg reflector (DBR) lasers [12] are primarily designed for optical communication and use integrated gratings to achieve single mode operation. They are very compact and easy to operate, but their wavelengths are usually limited to 1.3 μm and 1.55 μm where the transmission loss of optical fibres is minimum. DFB lasers and DBR lasers at other wavelengths are rarely available and expensive. External cavities to force Fabry-Pérot (FP) type lasers to operate in a single mode are widely used for spectroscopic work [13]. Grating based external cavity diode lasers offer narrow linewidth ($\approx$ 100kHz) output which is very useful for probing atomic transitions. Reviews of application of diode laser in atomic physics are given by Camparo [14] and by Wieman and Hollberg [4]. Short external cavity lasers are also used in trace gas detection [15]; they are easy to construct, compact, and inexpensive.

Broad spectral coverage or tunability in semiconductor lasers is another highly sought after feature for spectroscopic applications. To detect trace species, the wavelength of the diode laser has to be coincident with an absorption line and must be tuned on-off the line to sense the difference in absorption. The central wavelength of diode lasers are decided by their material, e.g., devices that operate in the 0.67 μm spectral region are based on InGaAlP, devices in the 0.75-0.98 μm spectral region are based on AlGaAs and InGaAs [4], devices in the 1.2-1.6 μm spectral region are based on InGaAsP/InP, devices in the 1.6-2.3 μm spectral region are based on an InGaAs/InGaAsP system [16], and Pb-salt diode lasers operate in a range of 2-30 μm [10]. In the quaternary and ternary systems the emission wavelength of the laser is set by the composition. The tunable range for each laser is from a few nm to a few tens of nm depending on the tuning schemes.

1.2 Trace Gas Detection with Diode Lasers

High sensitive monitoring of trace gas has become increasingly important as a direct result of concerns over causes and effects of atmospheric pollution. Many molecules have vibration transitions in the near-infrared (NIR) and middle-infrared (MIR) regions. The HITRAN [17] database lists extensive information such as line strength, line centre wavenumber, linewidths and pressure broadening parameters for atmospheric molecules. The absorption lines in the MIR region are fundamental rotational or vibrational transitions. They are orders of magnitude stronger than the vibrational overtone transitions in the NIR region and permit an order of magnitude higher detection sensitivity. But the MIR region

can only be accessed by Pb-salt diode lasers which presently require cryogenic cooling and much more injection current. Today the NIR diode lasers are far more technologically advanced and economical than Pb-salt devices as a result of a tremendous research effort driven by the telecommunication industry. To achieve high-sensitivity detection in the NIR region, a variety of modulation techniques have been investigated [18][19][20][21] [22][23][24][25]. These methods can be divided into two groups according to the modulation frequency: one- and two-tone frequency modulation (FM) techniques in which the modulation frequency is of the same magnitude as the absorption linewidth, with reported sensitivities of the order of 1×10^{-7}-1×10^{-8} fractional absorption [26][27][28][29][30], and wavelength modulation (WM), performed at frequencies that are substantially less than the absorption linewidth, with sensitivities of 1×10^{-4}-4×10^{-6} [31][32][15][33][34][35][36]. Many investigations have been performed to demonstrate the use of NIR diode lasers in trace gas detection. Table I lists some important molecules and projected sensitivities in the NIR region [7].

1.3 Trace Liquid Detection with Diode Lasers

Many materials in chemistry or industrial quality and process control are in a liquid state and have absorption peaks in the NIR and MIR region. Traditional optical measurements are performed by Fourier-transform infrared (FT-IR) spectrometers which are bulky and expensive. There is a need for a quick, compact, and inexpensive method of liquid detection

Mol.	Wavelength λ (μm)	Line Strength S($cm^2 \cdot mol^{-1} \cdot cm^{-1}$)	Line width γ (cm^{-1})*	Sensitivity (ppm-m)**
CH_4	1.651	8.7×10^{-22}	0.05	0.07
CO	1.567	2.3×10^{-23}	0.066	3.6
CO_2	1.573	1.6×10^{-23}	0.06	4.7
HBr	1.341	2.1×10^{-23}	0.08	4.8
HCl	1.747	1.2×10^{-20}	0.092	0.01
HF	1.330	1.3×10^{-20}	0.033	0.003
HI	1.541	3.1×10^{-22}	0.06	0.24
H_2O	1.365	2.1×10^{-20}	0.095	0.006
H_2S	1.578	1.3×10^{-22}	0.175	1.7
NH_3	1.544	3.7×10^{-22}	0.06	0.2
NO_2	0.800	5.0×10^{-23}	0.073	1.8
O_2	0.761	7.7×10^{-24}	0.056	9.1

* Air-broadened half width γ at 1 atm
** Concentration-pathlength Cxl of the given molecule that could be detected with a S/N ratio of one in a 1 Hz bandwidth for a 10^{-6} absorption sensitivity.

and identification. However, there appears to be little activity in the application of diode lasers to the detection of liquids even though available wavelengths from diode lasers in several different material systems can cover the NIR region from 0.7 to 2.5 μm. This is because the spectral features in the liquid state are much broader than the analogues in the gaseous state [37], and the spectral coverage provided by temperature or current tuning of diode lasers is not adequate to perform reliable liquid detection and identification. Another difficulty in general with NIR spectroscopy is the lack of structural interpretative values compared with MIR spectroscopy. Many overtone bands related to O-H, C-H, and N-H groups fall within this region and thus the spectrum of even a simple mixture is the sum of several bands that overlap.

The development of chemometrics in recent years has significantly changed the outlook

of NIR spectroscopy [38]. Calibration methods based on a principal [illegible] (PCR) and a partial least-squares (PLS) analysis yield good predictions for mixtures and even for biological samples that have complex spectra. In recent years there has been activity in the applications of NIR spectroscopy as an analytical tool to replace traditional slow, wet chemical methods in process control, the food industry, and noninvasive medical analysis [39].

A multiple short external cavities (MSXC) scheme to force diode lasers to operate on 18 distinct modes with a spectral coverage of 72nm was developed and is reported in this thesis [40]. This spectral coverage was achieved at constant current and room temperature and is considerably greater than the $\approx$ 10nm tunable range achieved by a DFB with a $\Delta T = 100°C$, or the $\approx$ 35nm single mode spectrum coverage offered by a short external cavity laser with a $\Delta T = 130°C$ [15]. The MSXC technique greatly facilitates the application of diode lasers in liquid detection, and provides an opportunity to combine the advantages offered by diode lasers with the predictive ability of the multivariate analyses, e.g., PLS and PCR modelling.

Some novel integrated tunable diode lasers such as micro-machined external cavity laser or sampled grating DBR lasers have been reported recently [41][42]. These lasers can be tuned over a few ten nm and are primarily designed for wavelength domain multiplex (WDM) telecommunication. As has happened with NIR diode lasers used in gas state detection, the lasers designed for WDM can be used in liquid detection after they become

widely available.

1.4 Goal and Outline of the Thesis

The goal of the research reported in this thesis was to study schemes to achieve single mode operation with wide tunability, which includes the use of short external cavity, multiple short external cavities and grating external cavity, and to apply tunable lasers in sensitive trace gas and trace liquid detection. The development of the MSXC lasers and the GEC lasers, and comparison among the SXC lasers, the MSXC lasers and the GEC lasers are described in Chapter 2. In Chapter 3, trace gas detection by diode lasers and an analysis of the harmonic content in modulation spectroscopy with a semiconductor diode laser under injection current modulation are reported. An electronic subtracter scheme was developed to achieve high sensitivity by subtracting the excess laser noise. In Chapter 4 applications of MSXC lasers in liquid detection are summarized. A phase sensitive detection scheme and wavelength discrimination method are described. The PCR and PLS were used to process the multiwavelength data. The performance of liquid detection is studied in the system of H_2O in D_2O and in a three mixture system of H_2O, acetone and methanol. Chapter 5 describes the design of a broad gain peak multiple quantum well laser and initial results on the performance are presented. Finally, the results of the thesis and topics for future research are summarized in Chapter 6.

The work in this thesis has been presented at CLEO'96 conference [43] and accepted

by Optoelectronics 97 conference [44] and reported in four publications [45][46][47].

CHAPTER 2 - Operation and Construction of Tunable Single-Mode Diode Lasers

2.1 Introduction

Single mode operation and a large tunable range are two key features in the application of semiconductor diode lasers in the detection of trace species. Although Fabry-Pérot diode lasers are compact, easy to operate, low cost and available for many different wavelengths, they typically operate multimode and only have a limited tunable range by varying temperature or injection current. External cavity lasers retain, in large measure, the merits of solitary cavity diode lasers and in addition provide an improved performance in terms of single mode operation and tunability. There are many types of external cavity lasers; the choice depends on the specific applications. In this chapter the theory, construction and characteristics of a MSXC laser and a GEC laser are described. The qualitative operation of the external cavity lasers is explained by considering the effect of the external cavity on the reduced loss of the solitary laser. The basic design and construction of a MSXC and a GEC are given. The performance of a SXC laser, a MSXC laser and GEC laser is reported and compared in terms of side mode suppression ratio (SMSR), tunable range, stability and ease of construction and operation.

A lasing action requires both optical gain and optical feedback. Diode lasers consist of layers of epitaxially-grown semiconductor that form a p-n junction [47][48]. Forward biasing the diode laser creates an electron-hole population inversion and thus produces optical gain in the active region which is a very thin layer ($\sim 0.1\ \mu$m) located between highly doped p and n-type semiconductor. The active region confines charge carries because it has a smaller band gap than that of surrounding semiconductor layers, as well as photons because it has a higher refractive index than that of the surrounding layers. Optical feedback is provided by the interface formed by the cleaved facets and air with a reflectance of 0.32 for InGaAsP lasers.

A schematic representation of a Fabry-Pérot type diode laser with a length of active region L_d, facet reflectivity coefficients r_1 and r_2, and net gain (gain minus loss) g_d for electric field is as shown in Fig. 2.1(a), and if one ignores the contribution from the spontaneous emission, then the round-trip condition for steady-state laser operation, which requires no change in the amplitude of the electric field after one pass through the cavity, is [47]

$$r_1 r_2 \exp(g_d L_d - 4\pi i n_d L_d/\lambda) = 1, \tag{1}$$

where n_d is the effective refractive index of the active region. Equating the real parts of Eq. (1) gives the threshold condition

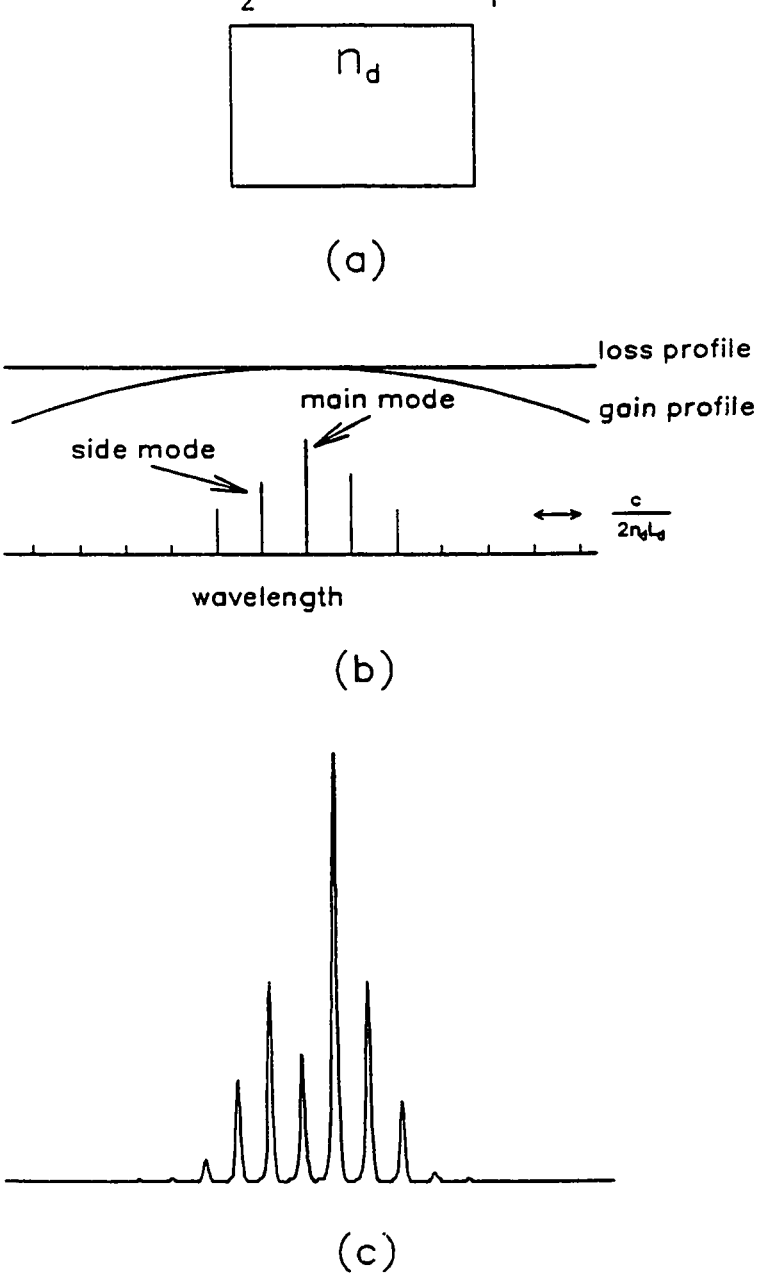

Fig. 2.1 (a): A schematic representation of a Fabry-Pérot type laser. (b): An illustration of the gain, the loss and the laser cavity modes as a function of wavelength in a Fabry-Pérot type laser. (c): A spectral output from a Fabry-Pérot type laser, the mode spacing is ≈ 1 nm for a 250 μm long laser.

$$g_d = \frac{1}{L_d} \ln(1/r_1 r_2) . \quad (2)$$

Once this threshold gain is reached by sufficient carrier injection, lasing begins and the gain is "clamped" at the threshold value. Equating the imaginary parts of Eq. (1) gives the multiple frequency solution

$$\nu_m = \frac{mc}{2n_d L_d}, \quad (3)$$

and the separation of the laser modes

$$\Delta\nu = \frac{c}{2n_g L_d}, \quad (4)$$

where m is a positive integer and n_g is the effective group index of the active region.

In the above description of diode lasers, many mechanisms which affect diode laser spectrum such as the spontaneous emission, spatial and spectral hole burning are not included. Due to these effects InGaAsP diode lasers normally operate above threshold with several longitudinal modes. Illustration of the net gain, loss and cavity modes and a measured spectrum from a 250 μm long InGaAsP index-guided laser are found in Fig. 2.1(b) and 2.1(c).

Multimode operation is undesirable for spectroscopic applications. One solution is to use a grating to feedback a specific wavelength chosen by setting the grating angle. Fig. 2.2(a) shows a grating external cavity in Littrow configuration. If the gain profile

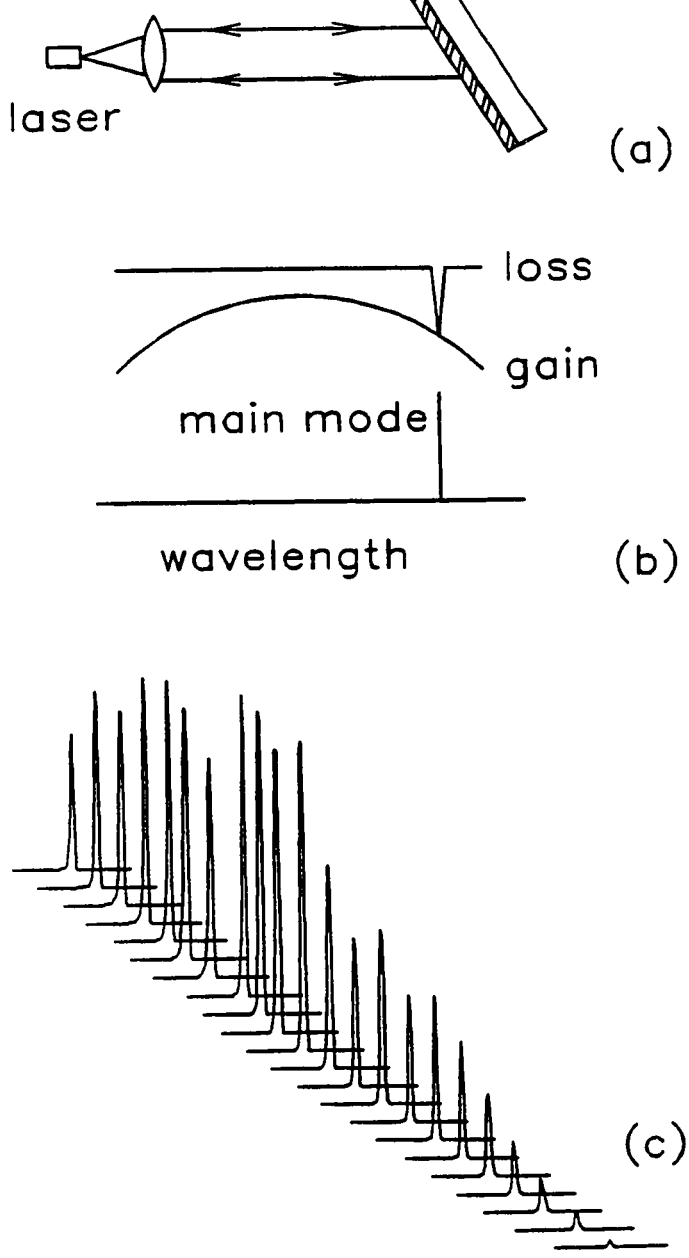

Fig. 2.2 (a): A schematic representation of a GEC laser. (b): An illustration of the gain, the reduced loss and the enhanced main mode in a GEC laser. (c): Spectral outputs from a GEC laser. The mode spacing between each of the 22 distinct modes is $\approx$2 nm.

is approximated by a parabolic function as shown in Fig. 2.2(b)

$$g(\lambda) = g_0 - k(\lambda_0 - \lambda)^2, \tag{5}$$

where g_0, k, and λ_0 are the gain at the wavelength of the peak, the gain width coefficient, and the wavelength of the gain peak, then the lasing wavelength λ_l corresponds to the point where the dip of reduced loss intersects the gain curve. If the dip is too far from the gain centre and can not reach the gain curve, the laser will lase at gain centre wavelength. The maximum tunable range $\Delta\lambda$ is given by [48]

$$\Delta\lambda = 2\left(\frac{1}{L_d k}\ln\frac{r_L + r}{r_L + r_L^2 r}\right)^{1/2}, \tag{6}$$

where r is the lumped reflection coefficient for a single pass in the external cavity, which includes the efficiency of the lens and the grating, and coupling between the laser and the external cavity. r_L is the amplitude reflectivity of the facet near the lens side. One can see that $\Delta\lambda$ is decided by the coupling efficiency of the lens and the laser, the grating reflection efficiency, the length of the laser, reflectivity of the laser facet and the flatness of the gain peak. Fig. 2.2(c) shows an example of spectra obtained from an InGaAsP laser with a grating external cavity. A total of ~40 modes are obtained (shown as the every other mode) and the spectral coverage is about 40nm.

2.3 Short External Cavity Diode Lasers and Multiple Short External Cavity Diode Lasers

The effect of feedback on the control of modes of a diode laser from a short external

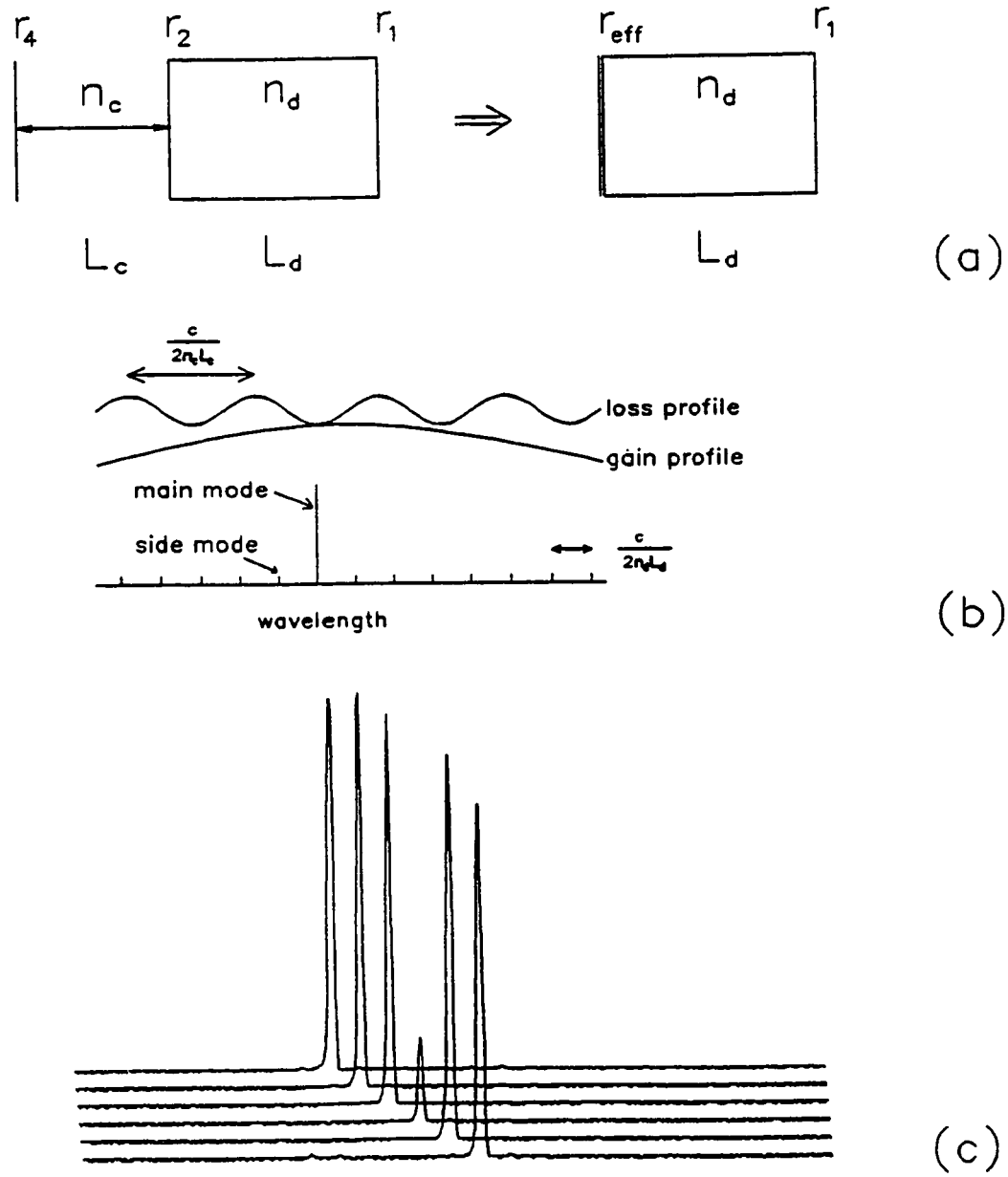

Fig. 2.3 (a): A schematic representation of a SXC laser. (b): An illustration of the gain, the modulation of the loss and the enhanced main mode and side modes in a SXC laser. (c): Spectral outputs from a GEC laser, the mode spacing between each of the 6 distinct modes is ≈ 1 nm.

cavity has been well studied [49][50][51]. It can be modelled conveniently by an effective reflection facet. If the reflection coefficient of the external cavity is r_4 which taking account the couping efficiency in Fig. 2.3(a), then the effective reflection coefficient is

$$r_{eff}=\frac{r_2+r_4 e^{(g_c L_c - 4\pi i L_c n_c/\lambda)}}{1+r_2 r_4 e^{(g_c L_c - 4\pi i L_c n_c/\lambda)}}, \qquad (7)$$

where L_c and n_c are the length and the refractive index of the external cavity, λ is the laser wavelength and g_c is total gain in the external cavity. Equation (7) includes multiple reflections for modelling very short external cavities.

The dependence of r_{eff} on L_c and λ induces a variation on the loss profile given by

$$\Delta\alpha=\frac{1}{L_d}\ln\left(\frac{r_1}{r_{eff}(L_c,\lambda)}\right), \qquad (8)$$

which enables the SXC scheme to select different FP modes. This mechanism of mode selectivity can be understood by referring to Fig. 2.3(b). The main mode selected by the SXC is the FP mode that has the lowest cavity loss and is closest to the peak of the gain profile. When L_c is changed by $\lambda/2n_c$ the output will cycle once over all possible modes. In practice, there is a limited usable range of L_c to have a maximum suppression of the adjacent side-modes. A small L_c, on the one hand, decreases the curvature of the modulated loss so that the net gain difference of the main mode and the side-modes is reduced. On the other hand, a small L_c will increase the amplitude of modulation loss due to increased feedback and will increase the net gain difference. As a rule of thumb the best trade-off is obtained when $L_c \approx n_d \times L_d/4n_c$ [47].

mode with a simple SXC. A small L_c is required to obtain the modes far away from the gain peak, but a flat curvature of the modulated loss due to a small L_c will inevitably cause a multimode operation. It is known that mode structure is very sensitive to the gain difference. A modulation loss of 1-5cm^{-1} suffices for a side mode suppression ratio(SMSR) of 20-30dB [47][48]. Fig. 2.3(c) shows the spectral output of an SXC laser for 6 different lengths of the SXC selected by changing the length of external cavity.

Based on the understanding of the mode selection mechanism in the SXC scheme, we have developed the concept of the MSXC to overcome the limitation in the SXC and to obtain broader spectral coverage. In the MSXC scheme there are two short external cavities as shown in Fig. 2.4(a). The first external cavity has a length of $L_e \approx n_d \times L_d/4n_e$, where n_e is the refractive index of the first cavity. The second external cavity has a length about $\sim 10\ \mu m$. The feedback from the second cavity defines the region where the main mode is located in the gain profile, while the feedback from the first cavity provides resonant enhancement to suppress the side modes around the main mode. Therefore single mode operation on modes far from the centre of the gain peak can be forced. In Fig. 2.4(a) the first cavity has a reflectivity coefficient r_3 and a total gain g_e, the second cavity has a reflection coefficient r_4 and a total gain g_c. We can apply the similar concept of effective facet to these two cavities [12] by writing two effective reflection coefficients as

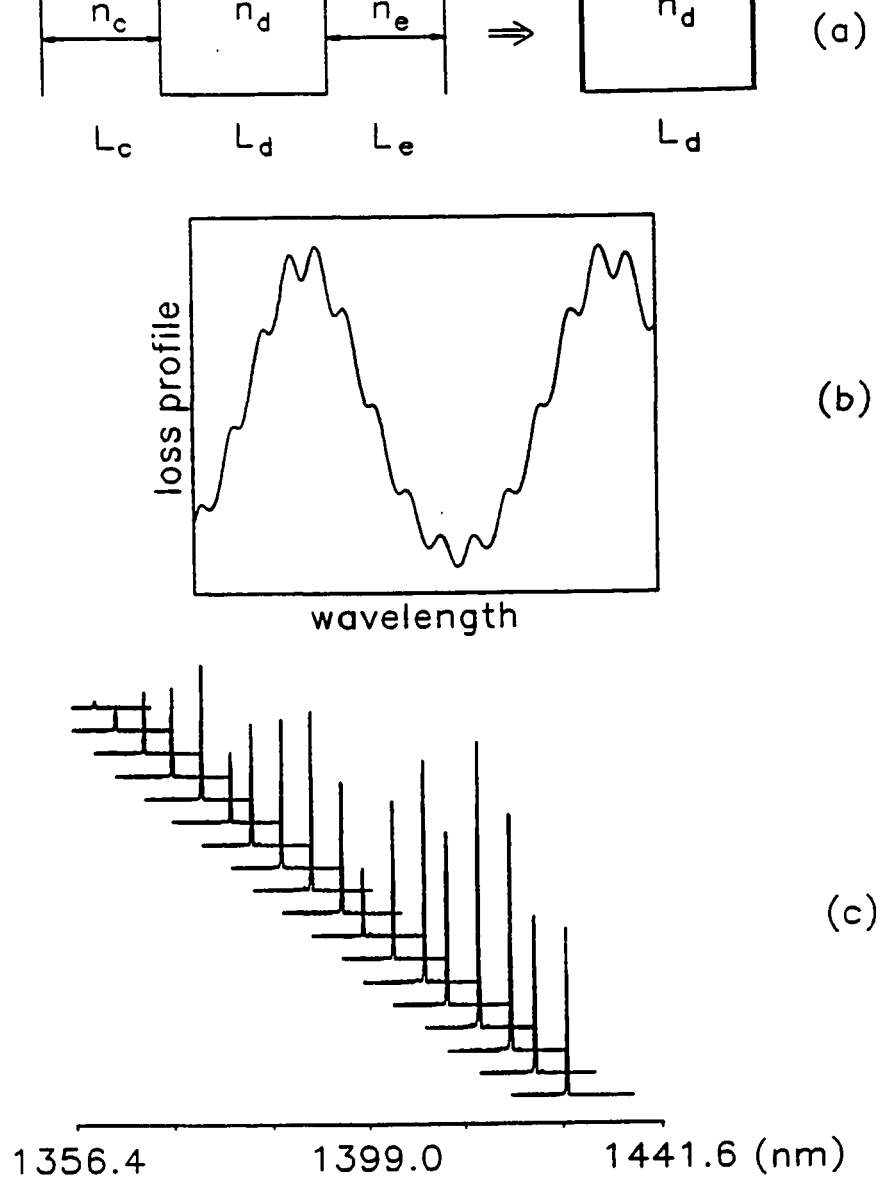

Fig. 2.4 (a): A schematic representation of a MSXC laser. (b): A calculated curve of the reduced loss a MSXC laser. The feedback from the second cavity determines the lasing region on the gain curve, the feedback from the first cavity sharpens the dip of the reduces loss and confines the laser in single-mode operation. (c): Spectral outputs from a MSXC laser, the mode spacing between the 18 distinct modes is $\approx$4nm.

$$r_{1e}=\frac{r_1+r_3 e^{(g_e L_e - i4\pi n_e L_e/\lambda)}}{1+r_1 r_3 e^{(g_e L_e - i4\pi n_e L_e/\lambda)}}, \tag{9}$$

$$r_{2e}=\frac{r_2+r_4 e^{(g_c L_c - i4\pi n_c L_c/\lambda)}}{1+r_2 r_4 e^{(g_c L_c - i4\pi n_c L_c/\lambda)}}, \tag{10}$$

the round-trip condition for the MSXC laser can be written as

$$r_{1e} r_{2e} \exp(g_d L_d - i4\pi n_d L_d/\lambda) = 1. \tag{11}$$

The variation on the loss profile can be calculated for given L_c and λ by

$$\Delta\alpha = \frac{1}{L_d} \ln\left|\frac{r_1^2}{r_{1e} r_{2e}}\right|. \tag{12}$$

In the external cavity regions, there is no active medium and no absorption loss. But not all light reflected goes back to the active region of the laser and interacts with the electrons because of diffraction loss. Bonnell and Cassidy [52] have found that the faction of light reflected back to the laser is less than 10^{-3} for a short external cavity. Several other workers [53][54][55] have also estimated the amount of light fedback to the laser. The accurate value depend on the dimension of the laser waveguide and is difficult to obtain. We have used g_e and g_c as parameters to estimate the diffraction loss. An example of the calculated variation on loss profile is shown in Fig. 2.4(b).

The mode selection mechanism in an MSXC laser can be understood by examining Fig. 2.4(b). When L_c is changed, the minimum loss dip is not moved to the next adjacent

by the etalon effect induced by the first external cavity. In this way, the laser will operate on one mode and then will hop to a mode that is spaced 2-4 free-running laser modes away as L_c is changed. The lasing modes are the modes enhanced by the etalon effect of the first external cavity and the spacing is decided by L_c. The modes far away from gain peak can be forced to lase in a single mode without suffering a poor SMSR due to the flat curvature of loss modulation, because the etalon effect sharpens the loss modulation peak. An example of spectral outputs from a MSXC laser is shown in Fig. 2.4(c). In this case the spacing between the lasing modes is 4 free-running laser modes.

2.4 Construction and Operation of External Cavities Lasers

2.4.1 Grating External Cavity Lasers

Many configurations of grating external cavity lasers have been used [13]; the goal of our design is to make a stable, simple and compact module. Fig. 2.5(a) shows the picture of the design. It consists of two components, each piece is an independent flexure mount and is made of brass to provide the required flexibility. The laser chip is glued to a copper block with a thermistor(YSI 44006). A Peltier cooler (Melcor FC 0.45-32-05L) is sandwiched between the copper block and the laser block. A diffraction limited lens (350230-C, THORLABS) which is glued on the base focuses the beam on the grating and refocuses the reflected beam back to the laser. A fine thread screw (F25SS-038, THORLABS) on the back base can be used to adjust the angle of feedback beam within a range of $\pm 1.2°$.

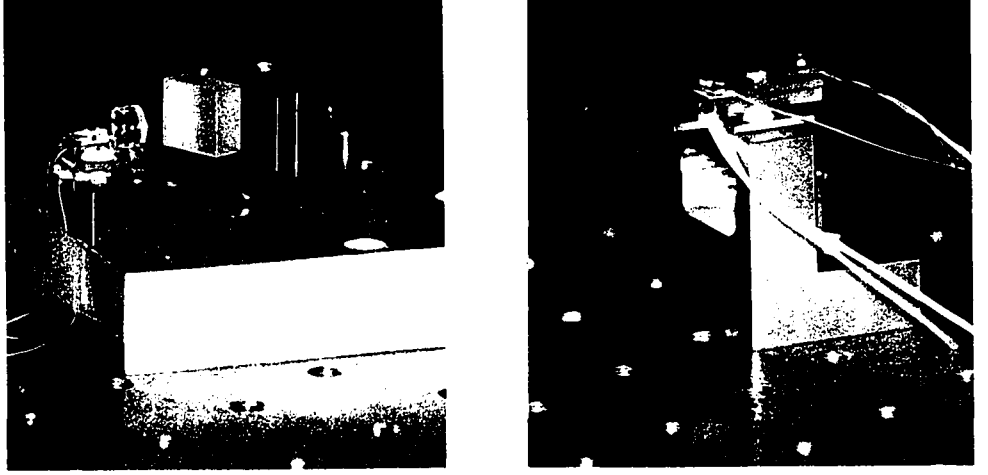

(a) (c)

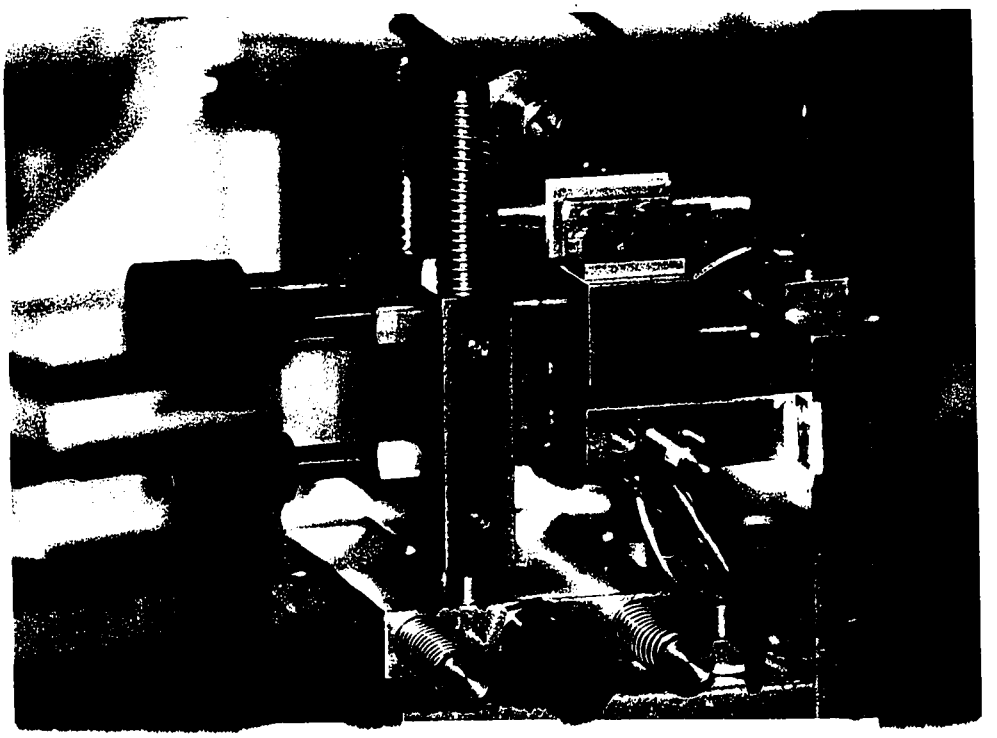

(b)

Fig. 2.5 (a): A picture of the compact GEC laser. (b): The 5-axis stage designed for study of the MSXC scheme. (c): The compact MSXC laser for sensor applications. See text for details.

The second flexure mount can be screwed on the base with the required angle. The grating (600 line/mm, blaze angle of 22.01° at 1.25 μm, ruled grating, E43746, Edmund Scientific) is glued on the second mount. Fine tuning, in the range of $\pm 0.5°$, is achieved by the second fine thread screw (F25SS-038, THORLABS).

2.4.2 Multiple Short External Cavities Laser

The SXC scheme has been implemented and successfully used for trace gas detection [11]. In those experiments the distance between the mirror and the laser was ≥ 150 μm. To achieve a large tunable range in the MSXC, the rear mirror, which functions as the second cavity, has to be positioned close to the laser(~ 10 μm). This is difficult to do with the previous mount. To overcome this difficulty a 5-axis stage as shown in Fig. 2.5(b) was designed. This stage can hold the assembly of the laser, the thermistor (YSI 44006) and the cooler (Melcor FC 0.45-32-05L). It also provides a platform to hold the piezoelectric transducer (PZT, AE0203D08, NEC or P-171, Physik Instrument) and provides xyz motion, tilt, and rotation to align the feedback surface parallel to the laser facet and control the coarse distance from the laser. Because very fine adjustment screws (80 threads per inch, FAS175 and FAS300, THORLABS) were used to position the PZT, the mirror can be put very close to the laser facet. The first cavity for single mode confinement feedback is provided by a thin glass plate (150 μm, No.1, Corning Cover Glass) which was held(by an index matching grease, Q2-3067 optical couplant, Dow Corning) to the front of the laser.

The 5-axis stage was designed to study the performance of the MSXC scheme and test new lasers in the lab environment. To make the MSXC laser more suitable for sensor application, a compact and rugged MSXC laser by using a smaller PZT was made, which required no adjustment during the operation. The PZT (AE0203D08, THORLABS) had a displacement of 6.5 μm for 100V and a size of $0.2\times0.3\times1.0cm^3$ and was glued down on the copper block that holds the laser chip. This MSXC configuration is rugged and stable; it essentially eliminated any mode hops caused by table vibrations or acoustic noise. A thermistor (YSI 44006) was epoxied in the copper block for temperature feedback. All of the above components plus a Peltier cooler (Melcor FC 0.45-32-05L), which was underneath the cooper block for temperature control, had a size of $1\times2\times3.5cm^3$.

2.5 Comparison of Different Type of External Cavity Lasers

The GEC, SXC and MSXC have different features and the choice of which one to use depends on the application. It is useful to compare them in terms of general functions and operations. Table II gives a comparison among the external cavity lasers. DFB lasers are included because they are often found in spectroscopic applications. There are many ways to construct each scheme. Table II is only a list derived from experience in operation or construction of these diode lasers. The lasers were all ridge wave guide lasers.

DFB lasers operate single mode and are very easy to use but their wavelengths are limited around 1.31 μm and 1.55 μm and tunable ranges are small. Even though some

	DFB	GEC	SXC	MSXC
tunable range:	⟨10nm	20-100nm	10-30nm	≈70nm
wavel. availab.:	limited	fair	fair	fair
SMSR:	excel.	excel.	good	moderate
tuning mechanism:	temp.	rotate grating	mirror +temp.	mirror +etalon
coverage:	conti.	conti.	conti.	$\Delta\lambda$~4nm
stability:	excel.	good	good	moderate
construct:	complex	moderate	easy	easy
operation:	simple	complex	moderate	moderate
cost:	high	high	low	low
application:	gas	gas	gas	liquid

other wavelengths have become available now, DFB lasers are usually very expensive. GEC lasers offer good single mode operation, wide tunable ranges, and available wavelengths. They also offer narrow linewidth. They are suitable for spectroscopy in laboratories, but automatically tuned GEC lasers are complicated in mechanics and expensive. SXC lasers can be easily constructed from Fabry-Pérot type lasers, so the available wavelengths are less limited. They are suitable for making low cost gas sensors. MSXC lasers are similar to SXC lasers, except they offer wider tunable range under the loss of complete spectral coverage. They are suitable to make low cost, compact liquid sensors which need to measure a broad spectrum at a few nm intervals due to a broad absorption feature.

2.6 Summary

The operation of SXC, MSXC and GEC lasers have been qualitatively discussed by an empirical model of a parabolic gain profile and a reduced loss. The constructions of MSXC and GEC lasers have been described. The performance of SXC, MSXC, GEC and DFB lasers were compared in terms of single mode operation, tunability, as well as ease of construction, stability, availability and cost. The DFB and SXC lasers described in this chapter have been used in the work of trace gas detection and injection current modulation spectroscopy that is described in Chapter 3. The MSXC lasers have been used in the work of detection of liquids which is summarized in Chapter 4. GEC lasers have been applied to the characterization of a diode laser with a broad gain peak, as reported in Chapter 5.

CHAPTER 3 - MODULATION SPECTROSCOPY AND TRACE GAS DETECTION

3.1 Introduction

Tunability, low cost, simplicity and cw operation at room temperature have made diode lasers widely used in laser absorption spectroscopy for trace gas detection [3][4][56][57][58][59][60][15]. Despite these advantages, the practical implementation of diode lasers is limited by excess noise, sensitivity to optical feedback, injection current fluctuations, and optical fringes. To achieve high-sensitivity detection, frequency modulation (FM) and wavelength modulation (WM) schemes are widely used in diode laser spectroscopy in which the detection sensitivity is maximized by narrowing the detection band and shifting the detection band to high frequency to avoid excess noise, i.e., 1/f noise. Although a similar strategy is employed in the two techniques, the techniques evolved from different origins. WM was used with lead-salt diode lasers by direct current modulation [61][19] and with a modulation frequency in the 1-100kHz range. FM spectroscopy was first employed by Bjorklund [18] in dye laser spectroscopy and an external electro-optic modulator was used with a modulation frequency in the GHz range. Since then variations on the methods have been developed, such as high frequency WM modulation [62][26], two tone WM modulation [21], one and two tone direct current FM modulation

variations have used near-infrared diode lasers which were developed for fibre-optic communication and have better performance in terms of linearity of the L-I curve, temperature of operation and threshold current [55][34], than Pb-salt diode lasers. Recently some workers [22][65] have shown that FM and WM can be considered in an unified frame and formalism, and that the distinction is that in FM the modulation frequency is of the same magnitude as the absorption linewidth whereas WM is performed at frequencies that are substantially less than the absorption linewidth.

The formalism for FM modulation is typically based on the concept that the electric field of the laser light is modulated [18]. It is the correct description for a laser with an external modulator [18][66][67][62][68], be it a dye laser, a solid state laser, or a diode laser. However, the formalism has lately been extended to FM spectroscopy with diode lasers employing current modulation [69][70][71][23][26][61][22], where it is the light intensity rather than the electric field that is directly modulated. By stating that the intensity is directly modulated we mean there is a linear relation between the modulation of the intensity and the modulation signal. For first harmonic (1f) detection the concept of FM based on a modulated electric field gives a correct result only if terms of second order or higher in the amplitude of the current modulation are ignored. Confusion about detected signals arises when second harmonic (2f) detection is considered. For example, there is a constant 2f background present according to the modulated electric field FM theory [22] even when there is no absorption.

Subtraction is another commonly used method to reduce the noise. The concept is that when a laser beam is split into a signal beam and a reference beam and both of them are detected by similar photodiode detectors, since the optical systems (lenses, beam splitter and detectors) exhibit excellent linearity and temporal bandwidth, a subtraction of the detector outputs of the signal and reference channels should cancel waveforms that are common to both channels. Thus it is possible to reduce, in the subtracted signal, contributions from diode laser noise, optical feedback, optical fringes, and the background signal.

In the first part of this chapter, we present an analysis for the modulation spectroscopy of a diode laser based on the concept that the light intensity is directly modulated by the injection current. We also show that 2f detection can be considered in an unified frame of FM and WM. Experimental confirmation is given by measuring 1f and 2f signals from a sinusoidally current modulated DFB laser and a 2f water vapour spectrum in WM. In the second part of this chapter, highly sensitive detection of water vapour is presented. A subtraction scheme to reduce the noise, background signal and dynamic range required of the lock-in amplifier for second harmonic (2f) detection in the 5-20kHz frequency range (wavelength modulation) is described. A 1.39 μm SXC laser is used with an electronic noise subtracter. A beam noise level (defined as 2$\times$ the rms value) equivalent to a line centre absorption of 1.6×10^{-6} was achieved with an ENBW of 1.25Hz for 2f detection at 10kHz.

3.2 Modulation Spectroscopy of Diode Lasers

3.2.1 Theory Overview

For an ideal diode laser each electron of the current above the number required to achieve threshold will create a stimulated photon. A reverse process happens in a photodiode where an absorbed photon will create an electron-hole pair. The photodiode is therefore called a square law detector because the resulting photocurrent is proportional to the square of the electric field of the light, i.e, intensity of light [72]. The process involving a photon and an electron-hole pair is linear in the current flowing in the diode laser and the current flowing through the photodiode. A perfect diode laser (i.e., one with a linear L-I curve) which is current modulated sinusoidally above the threshold will have a sinusoidally modulated light intensity. The detected photocurrent from a photodiode which is exposed to the laser beam will be a sinusoidally modulated signal.

Based on the above consideration, the electric-field amplitude of the perfect diode laser after direct current modulation at frequency ω_m can be written as

$$\begin{aligned} E(t) &= E_0 [1+M\sin(\omega_m t+\psi)]^{1/2} \exp(i\omega_0 t + i\beta\sin\omega_m t) \\ &= E_0 \exp(i\omega_0 t)[1+M\sin(\omega_m t+\psi)]^{1/2} \sum_{n=-\infty}^{\infty} J_n(\beta)\exp(in\omega_m t), \end{aligned} \tag{13}$$

where ω_0 and ω_m are the optical frequency and the modulation frequency, ψ is the phase difference between amplitude modulation and frequency modulation, and J_n is the nth-order Bessel function. M is the amplitude modulation index and is defined as the maximum excursion in light intensity ΔI divided by the time-averaged intensity I_0 (see Eq. 20). β

in the instantaneous frequency $\beta\omega_m$ with the modulation frequency ω_m. In WM, β is much larger than 1 and ω_m is much smaller than the width Γ of the spectral feature of interest, whereas in FM the modulation frequencies can be up to several gigahertz so that $\omega_m \gg \Gamma$ and β is usually less than 1.

By using expansions in Appendix A, Eq. (13) can be written as

$$E(t) = E_0 \exp(i\omega_0 t) \sum_{n=-\infty}^{\infty} r_n \exp(in\omega_m t), \tag{14}$$

where r_n is given by

$$r_n = \sum_{k=-\infty}^{\infty} a_k J_{n-k}(\beta), \tag{15}$$

$$a_0 = 1 - \sum_{j=1}^{\infty} \frac{1\cdot 3\cdot 5\cdots(4j-3)}{2^{4j}\cdot j!\cdot j!} M^{2j}, \tag{16}$$

$$a_k = -i^k \cdot e^{ik\psi} \left[\sum_{j=1}^{\infty} \frac{1\cdot 3\cdot 5\cdots(4j+2|k|+e-7)}{2^{4j+2|k|-4}(j+|k|-1)!\,(j-1)!} M^{2j+|k|-2} \right], \tag{17}$$

where $e=2$: *for* $k=\pm 1$ *with* $j=1$
$e=0$: *otherwise.*

After the laser beam passes an absorption sample with a complex transmission function $T(\omega_n)=\exp(-\delta_n - i\phi_n)$, where δ_n is the field amplitude attenuation and ϕ_n is the dispersion

$$E_T(t) = E_0 \exp(i\omega_0 t) \sum_{n=-\infty}^{\infty} T(\omega_n)\, r_n \exp(in\omega_m t), \tag{18}$$

and the transmitted optical intensity is then

$$I_T(t) = \frac{c}{8\pi} E_0^2 \sum_{n=-\infty}^{\infty} \sum_{n'=-\infty}^{\infty} T(\omega_n)\, T^*(\omega_{n'})\, r_n r_{n'}^* \exp[i(n-n')\,\omega_m t]. \tag{19}$$

This expression is valid for arbitrary modulation indices M and β and arbitrary line shapes δ_n and ϕ_n. Simplifications can be made for many cases such as small M, β and for weak absorption ($\delta_n, \phi_n \ll 1$) [61][63]. With a square-law photodetector, a signal that is modulated at ω_m and its harmonics can be coherently detected by a lock-in amplifier in WM or a radio frequency mixer in FM. By selecting the terms of $n' = n+q$ and $n' = n-q$ in Eq. (19), and $I_0 = cE_0^2/8\pi$ the qth harmonic signal is obtained as

$$I_q(t) = I_0 \exp(iq\omega_m t) \cdot \sum_{n=-\infty}^{\infty} r_{n+q} r_n^* \exp(-\delta_{n+q} - i\phi_{n+q} - \delta_n + i\phi_n) + c.c. \tag{20}$$

It is important to examine the residual amplitude modulation (RAM) background signal (when $\delta_n = \phi_n = 0$) in understanding the limitation of detection sensitivity [22][61][62]. By letting $\delta_n = \phi_n = 0$, using [73]

$$\sum_{n=-\infty}^{\infty} J_{n-k}(\beta)\, J_{n-k'}(\beta) = J_{-k+k'}(0) = \delta_{kk'}, \tag{21}$$

and Eq. (20), the RAM signals for different harmonics are given as

$$I_{RAM}=\begin{cases} I_0 & f=0 \\ I_0 M\sin(\omega_m t+\psi) & f=1 \\ 0 & f\geq 2 \end{cases} \qquad (22)$$

This result is expected from the square of Eq. (13). It is different from the results that assume that the electric field is directly modulated by the injection current [22]. Equation (22) is in agreement with the experience in 2f WM detection and helps to explain why 2f detection shows no signal when no absorption is present, and has better sensitivity than 1f detection. For two-tone modulation, a similar formalism can be obtained by using r_n in Eq. (16) in Cooper's equations [23]. It can be shown for two-tone modulation that the 1f RAM signal is proportional to M^2 and that the 2f RAM signal is zero for a diode laser with a perfect L-I curve.

3.2.2 Experimental Results and Discussion

It can be seen that the major difference between electric field modulation and intensity modulation is in 2f detection with large M, i.e., in the WM spectroscopy region. Therefore the concept of the intensity modulation is easier to verify in the WM regime. We used a 1.31 μm DFB laser to see the RAM signal response to the amplitude modulation index M. The laser had a threshold of 34mA at 22.0°C and its L-I curve is shown in Fig. 3.1(a). The laser injection current was biased at 50.6mA and modulated by a sine wave of amplitude 6mA at frequency of 5kHz. The light was detected by an InGaAs photodetector which was placed close to the laser facet to minimize distortion due to water absorption in the air. The waveform of sine current modulation signal as recorded with a digital oscilloscope

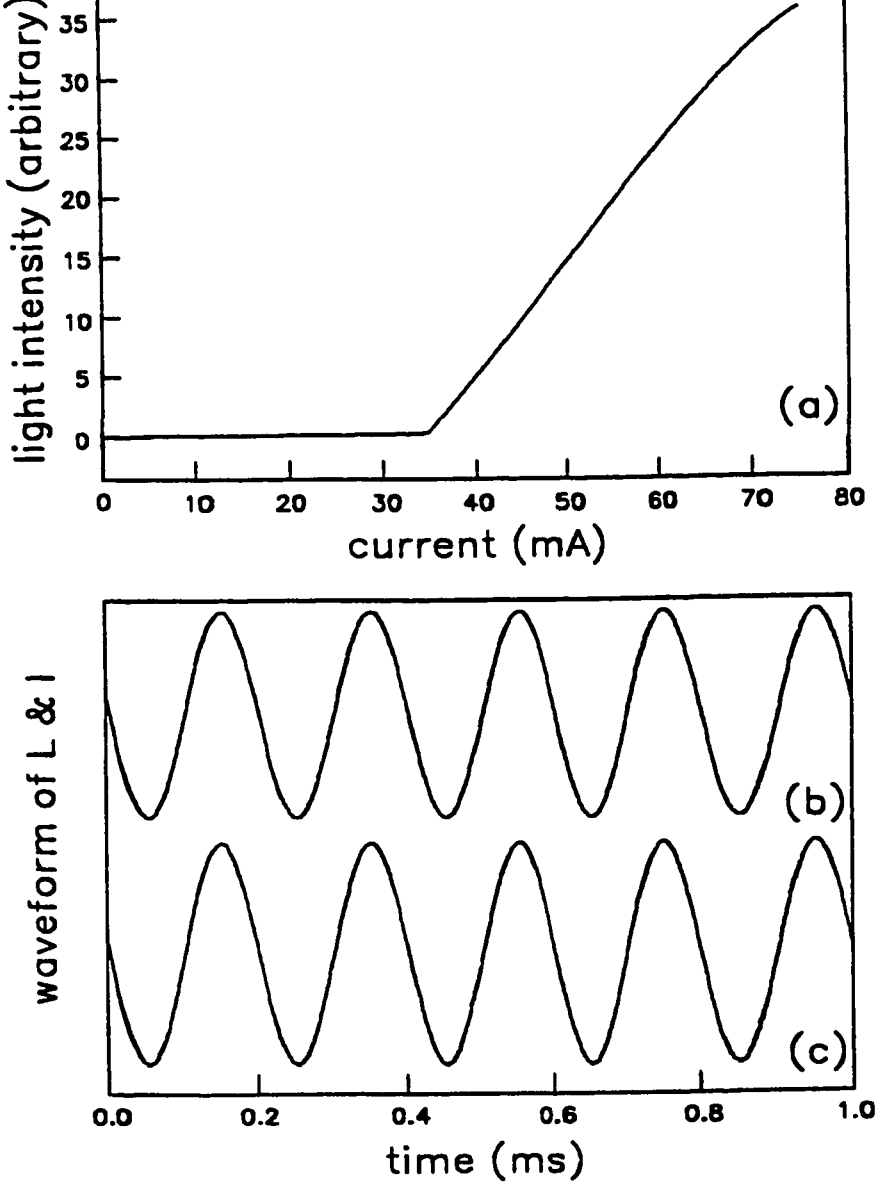

Fig. 3.1 The laser is biased at 50.6mA and sinusoidally modulated by the injection current in the linear portion of its L-I curve shown in (a). The sine waveform of current modulation with an amplitude of 6mA and the output from the photodetector are recorded by a digital oscilloscope and shown in (c) and (b) respectively. The sine waveform from the detector shows that the intensity of the laser light rather than the electric field is sinusoidally modulated by the injection current.

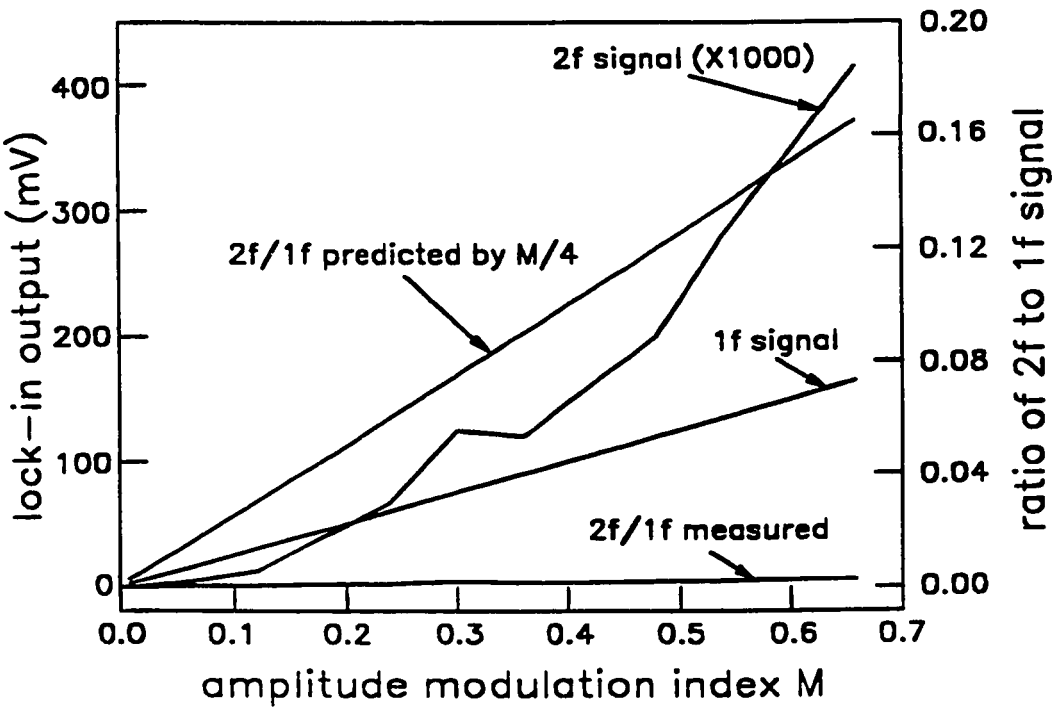

Fig. 3.2 1f and 2f signal from the lock-in amplifier and 2f/1f ratio verses the amplitude modulation index for a sinusoidal injection current modulation. Even including the contribution from the nonlinearity in the driving circuit and the L-I curve, 2f signal is close to zero. The measured 2f/1f ratio is also close to zero and far from M/4 predicted from a modulated electric field theory. Figure 3.2 shows the validity of the analysis of a modulated intensity discussed in the text.

wave with a voltage amplitude of 100mV. It is obvious that the intensity of the laser output is sinusoidally modulated. We measured 1f and 2f signals for different amplitude index M by a lock-in amplifier. Fig. 3.2 shows that the dependence of the 1f, 2f signal and the ratio of the 2f to 1f on M. According to Eq. 10, the ratio is zero, whereas in the concept in which the electric field is sinusoidally modulated by the injection current, the ratio is M/4 [22]. Fig. 3.2 shows that the ratio agrees with Eq. 10 and verifies that a modulation of the intensity is the correct description for diode laser spectroscopy with injection current modulation. The increase in 2f signal is caused by the nonlinearity of the modulation circuit and the nonlinear L-I curve of the diode laser as seen in Fig. 3.1(a). In FM region where the modulation frequency is close to the relaxation frequency of the diode laser, the response of the diode laser to the injection current modulation is more complicated, but we believe that direct modulation of the intensity by the modulation of the injection current should be the first order of approximation.

2f detection is almost invariably used in the WM spectroscopy, because the RAM background is essentially zero and the 2f signal has a peak at absorption line centre. From the above discussion one can see that the background (i.e., RAM) of 2f is essentially zero, which permits to use a more sensitive scale of a lock-in amplifier for a very weak absorption. In FM spectroscopy, 2f detection is rarely used because a very fast detector is required. To overcome nonzero background, two-tone FM is usually employed in which the background is proportional to the second order of M and the detection can be done in a much lower

frequency range (~MHz). 2f spectrum can be shown to have approximately a shape of the second derivative of the absorption line [74][9] in WM, while in FM the derivative feature is not very clear although the FM formalism is a more complete description in the sense that it includes the dispersion. We now show the FM and the WM can be unified for the case of 2f detection under the condition of M=0 for pure frequency modulation and weak absorption.

From Eq. (20), for M=0, r_n is replaced by J_n, and the second harmonic component is given by

$$\begin{aligned} I_{2f}=&2J_1J_{-1}\exp(-2\delta_0)\exp(-\delta_1-\delta_{-1}+2\delta_0)\cos(2\omega_m t-\phi_1+\phi_{-1}) \\ &+2\exp(-2\delta_0)\sum_{n=0}^{\infty}J_nJ_{n+2}[\exp(-\delta_n-\delta_{n+2}+2\delta_0)\cos(2\omega_m t-\phi_{n+2}+\phi_n) \\ &+\exp(-\delta_{-n}-\delta_{-n-2}+2\delta_0)\cos(2\omega_m t+\phi_{-n-2}-\phi_{-n})]\,. \end{aligned} \tag{23}$$

Because the sidebands (spacing ω_m) are very close to each other in WM, the absorption and dispersion difference for adjacent sidebands are therefore assumed to be constant $\Delta\delta$ and $\Delta\phi$, for the weak absorption, $|\delta_0-\delta_{\pm n}| = n\Delta\delta \ll 1$ and $|\phi_0-\phi_{\pm n}| = n\Delta\phi \ll 1$ for all n. By expanding $\exp(n\Delta\delta)$, $\cos(n\Delta\phi)$ and $\sin(n\Delta\phi)$ in Eq. (23) in a Taylor series and keeping the terms up to the second order of $\Delta\delta$ and $\Delta\phi$, Eq. (23) can be simplified to

$$\begin{aligned} I_{2f}=&2J_1J_{-1}\exp(-2\delta_0)[2\Delta\phi\sin(2\omega_m t)+(1-\Delta^2\delta-2\Delta^2\phi)\cos(2\omega_m t)] \\ &+2\exp(-2\delta_0)\sum_{n=0}^{\infty}J_nJ_{n+2}[2+2n(n+2)\Delta^2\delta-4\Delta^2\phi]\cos(2\omega_m t) \\ &+8\Delta\phi\exp(-2\delta_0)\sum_{n=0}^{\infty}J_nJ_{n+2}\sin(2\omega_m t)\,. \end{aligned} \tag{24}$$

By using [71]

$$J_1 J_{-1} + 2\sum_{n=0}^{\infty} J_n J_{n+2} = 0, \tag{25}$$

it can be seen that terms in first order of $\Delta\delta$ and $\Delta\phi$, and terms in second order of $\Delta\phi$ vanish in Eq. (24), which is consistent with the absence of dispersion information in WM, and the remaining terms of second order of $\Delta\delta$ term are

$$I_{2f} = 4\exp(-2\delta_0)\Delta^2\delta\cos(2\omega_m t)\sum_{n=0}^{\infty}(n+1)^2 J_n(\beta)J_{n+2}(\beta). \tag{26}$$

Furthermore the sum in Eq. (26) converges to $\beta^2/8$ [75] and $d\delta/d\omega = \Delta\delta/\omega_m$ for the small ω_m in the WM case. Finally, the 2f signal detected by a lock-in amplifier around the absorption line centre is

$$I_{2f} = \frac{\Delta\delta^2\beta^2}{2} = \frac{\Delta\delta^2\beta^2\omega_m^2}{2} = \frac{1}{2}\frac{d^2\delta}{d\omega^2}(\beta\omega_m)^2. \tag{27}$$

Eq. (27) is from a more rigorous treatment of 2f detection in the sense of including dispersion than the usual analysis in WM frame [19][9]. It shows why there is no dispersion signal {terms with $\Delta\phi$ vanish in Eq. (24)} and that the maximum variation on instantaneous frequency in WM theory can be shown as a product of frequency modulation index β and modulation frequency ω_m, and the 2f signal has a second derivative line shape.

The same DFB laser was used to detect water vapour over an 18m passlength with a pressure of 200 Torr. The output of the laser was sinusoidally modulated at 5kHz by modulation of the injection current and tuned by temperature. Fig. 3.3(a) shows the 2f

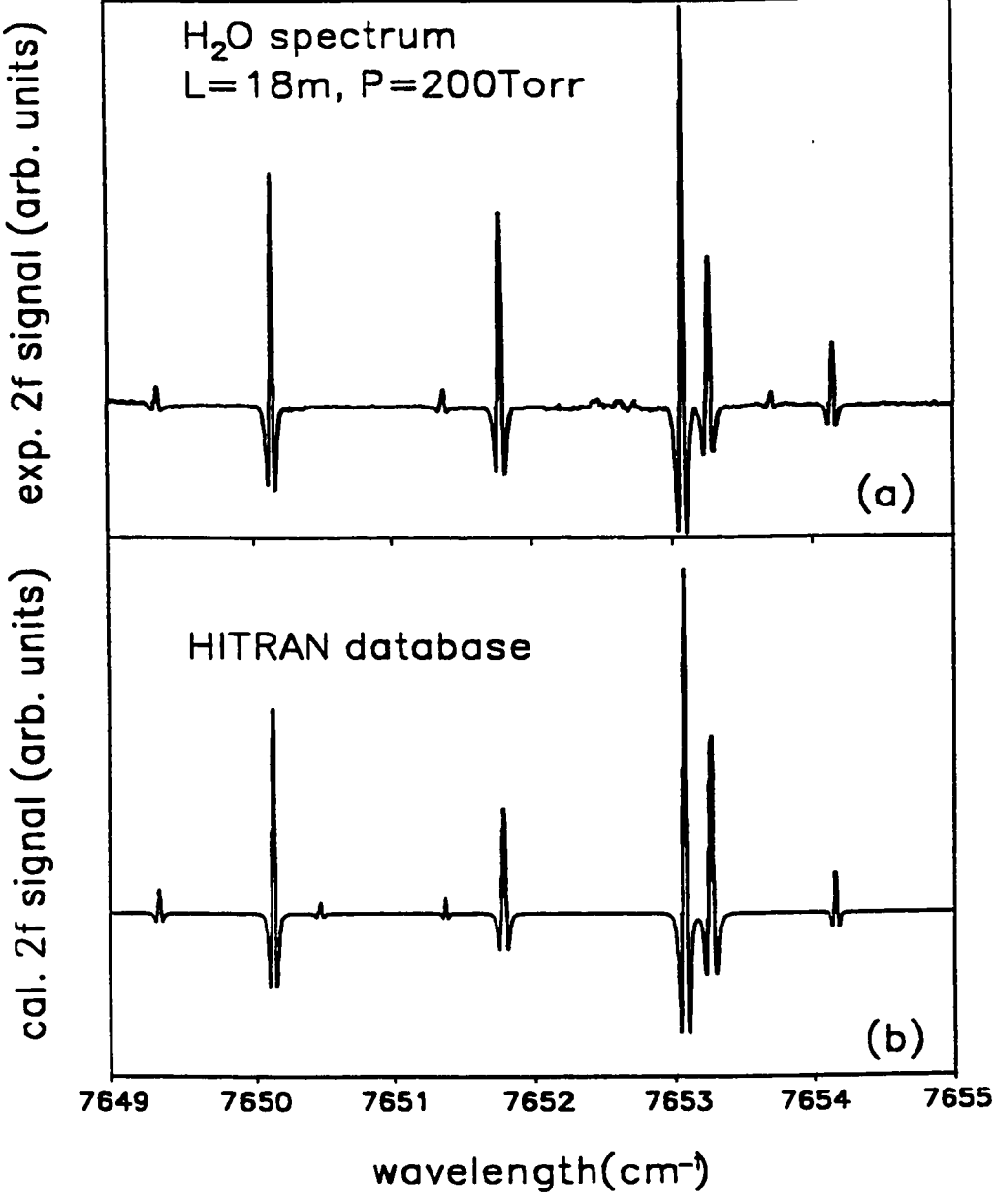

Fig. 3.3 2f H_2O spectrum measured at a pathlength of 18m and a pressure of 200 Torr. The same DFB laser is sinusoidally modulated by the injection current at 5kHz and its centre frequency is scanned by changing the temperature. The spectrum has a zero 2f background and a second-derivative absorption line shape.

spectrum recorded by a lock-in amplifier together with a 2f spectrum calculated from the HITRAN database [17] as shown in Fig. 3.3(b). The spectrum shows the typical feature in 2f WM detection, i.e., little 2f background signal and a second derivative line shape.

3.3 Highly Sensitive Detection of Water Vapour

3.3.1 Experimental Apparatus and Techniques

The experimental apparatus and detection electronics are shown schematically in Fig. 3.4(a) The noise subtracter, which is simple to build and inexpensive, automatically adjusts the subtraction ratio by using the difference between the DC photocurrents in a signal and a reference arms as a feedback signal and described in reference [43]. This scheme effectively reduces the signals common to both arms which includes optical feedback noise, optical fringes, and power supply pickup. In addition, the noise subtracter reduces the 2f background and reduces the dynamic range required of the lock-in amplifier by nulling the 1f intensity modulation signal. The performance of the subtraction scheme was tested with a 1.39 μm short external cavity (SXC) [15] laser. The SXC laser had temperature and current tuning rates of 0.3cm^{-1}/K and 0.05cm^{-1}/mA, respectively. The SXC systems allows the single mode operation of otherwise multimode lasers [15][32][33]. The laser light was collected by a singlet lens and two beam splitters were used to separate the output into three beams: a signal beam, a reference beam, and a beam for wavelength identification. The signal beam was routed through a White cell that was filled with water vapour and

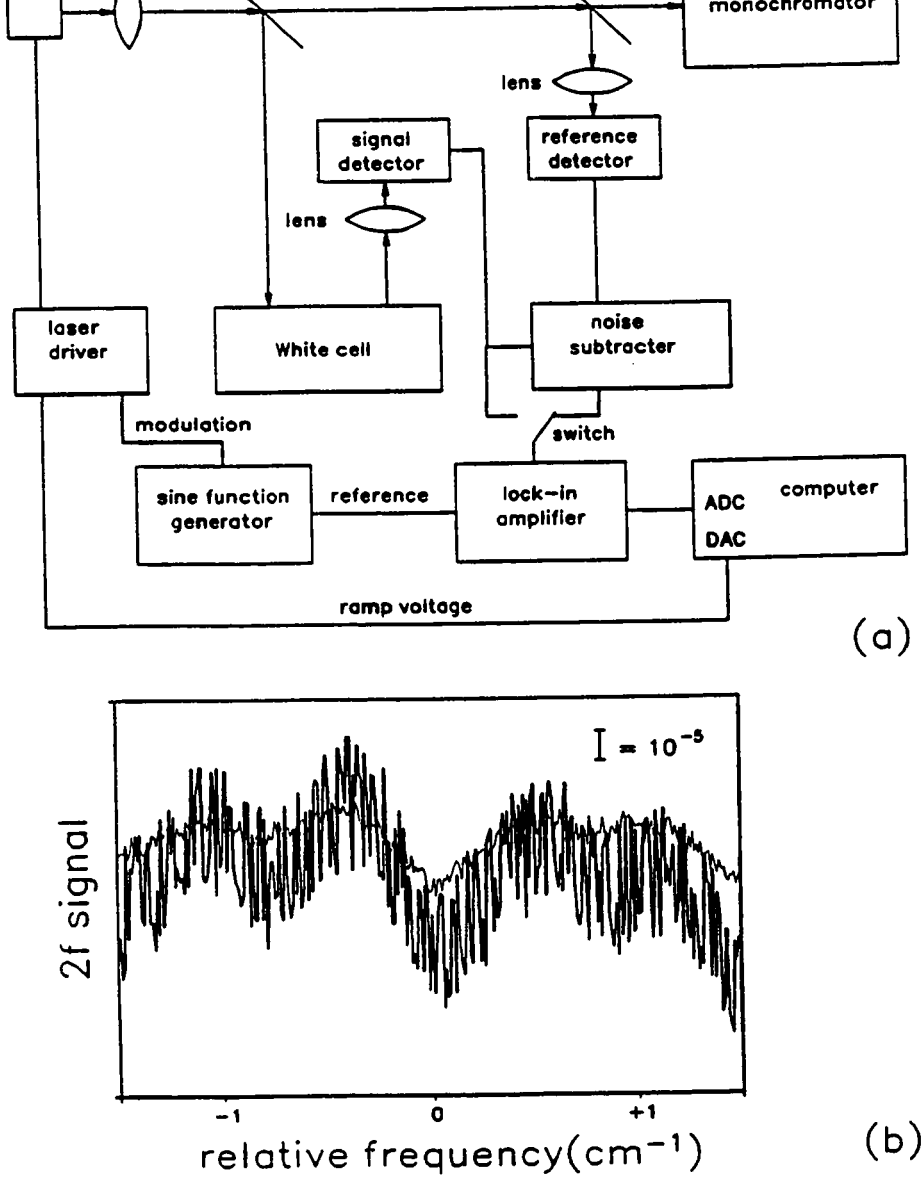

Fig. 3.4 (a): Schematic diagram of the apparatus used for second harmonic detection. The output from either the signal detector or from the noise subtracter could be directed to the lock-in amplifier. This allows results with and without the noise subtracter to be compared. (b): Spectral base-line scan with and without noise cancellation. The scans were obtained for 10 Torr water vapour in 200 Torr air. 17 dB noise reduction was achieved.

was set for a 4m pass length. With the exception of the path [illegible], the lengths of the signal and reference beams were approximately equal. All components in the optical path were carefully aligned in order to reduce the cause of optical feedback and fringes: the surface of detectors were tilted away from the optical axis by $>10°$ and the light was focused onto the detector material and not the surrounding case. All components were cleaned so that scattering was minimized.

The injection current was modulated by a sine wave at a frequency of 5kHz and second harmonic detection was used to obtain high sensitivity. The mean value of the wavelength of the laser was scanned by ramping either the injection current or the temperature of the laser. The outputs directly from the signal detector or from the noise subtracter were input into a lock-in amplifier, and the results were compared. To clarify different noise sources, we classify the noise into detector noise, beam noise, and modulation noise, and measure the noise level in terms of an equivalent absorption signal [32]. The modulation noise we take as $2\times$ the rms variation in the output of the lock-in amplifier in the absence of an absorption signal. The beam noise we take as $2\times$ the rms variation of the lock-in output when the current modulation for 2f is turned off. The detector noise we take as $2\times$ the rms variation in the output of the lock-in when the laser beam is blocked. To obtain the equivalent noise, $2\times$ the rms variation is normalized to the magnitude of the 2f absorption signal and multiplied by the peak absorbance of the absorption profile. Normally the detection sensitivity is limited by the modulation noise, usually due to optical fringes and optical feedback noise, before the photon shot noise limit is reached [76]. The implementation

of the noise subtracter effectively reduces the excess noise. To demonstrate reduction of modulation noise, the White cell was filled with $\approx$ 10 Torr of water vapour and 200 Torr air. Fig. 3.4(b) shows scans obtained from the signal detector and from the noise subtracter. The noise subtracter effectively reduced the modulation noise, as much as 17dB noise reduction was obtained in this scan.

3.3.2 Sensitivity of Absorption Detection

To determine the sensitivity, an absorption line with a weak but measurable direct absorption (i.e. 1-5% at line centre) was selected. The absorption was measured by detect detection (mechanical chopper) and by 2f detection. This provides a calibration of the amplitude of the 2f signal in percent absorption. The laser was then tuned to a nearby spectral region where there were no absorptions lines and the modulation noise, the beam noise, and detector noise were recorded.

An example of the noise levels obtained using the SXC laser is given in Fig. 3.5. The scan was taken at a total pressure of 35 Torr, 10kHz second harmonic detection with temperature ramp and an ENBW of 1.25Hz. Fig. 3.5(a) is the second harmonic signal with the largest absorption peak about $(5\pm1)\%$ absorbance. Fig. 3.5(b) is the scan in the same region with a more sensitive scale. The three traces in the inset are modulation noise, beam noise and detector noise. Two times the rms values of the scans are equivalent to absorptions of 2.7×10^{-6}, 1.6×10^{-6} and 6.2×10^{-7}, respectively. The beam noise, which

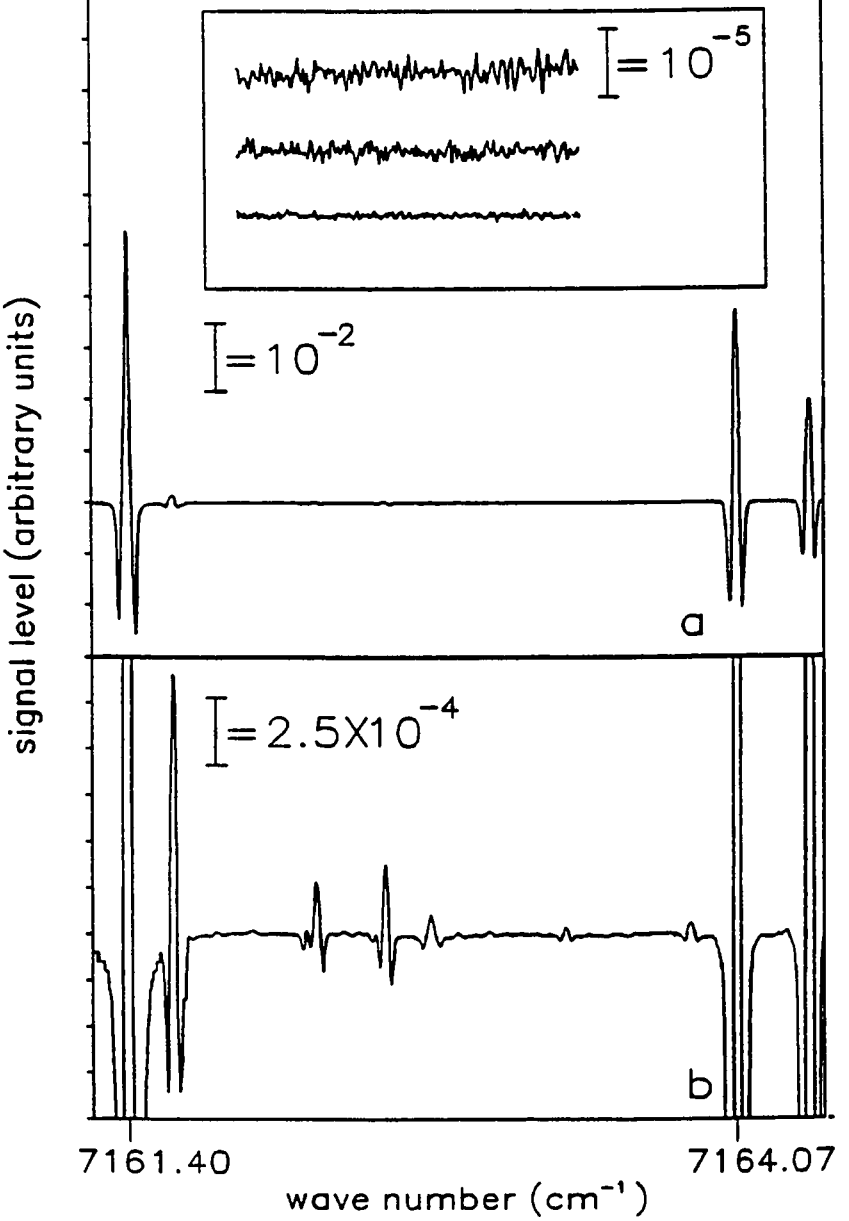

Fig. 3.5 Sensitivity of second harmonic detection using the subtraction circuit. (a), (b) are second harmonic scans of the water vapour lines at a total pressure of 35 Torr. The three traces in the inset, top to bottom, are modulation noise, beam noise, and detector noise (beam blocked), respectively. Two times the rms value of the beam noise is equivalent to an absorbance of 1.6×10^{-6} and is limited by the shot noise after noise cancellation.

ultimately decides the sensitivity of the second harmonic detection, is limited by the shot noise after noise cancellation, as is shown by a simple calculation of the shot noise based on the dc current in the detector.

3.4 Summary

The difference in FM and WM spectroscopy between a diode laser with an external modulator and a diode laser modulated by the injection current has been discussed. In the later case, it is the light intensity rather than the electric field that is directly modulated by the injection current. Formalism based on this concept has been developed and an unified frame for FM and WM in 2f detection has been given. 2f detection in WM is given to special attention because it has the larger difference between a directly modulated field and a directly modulated intensity. Experimental confirmation has been carried out by a 1.31 μm DBF laser in 2f WM detection.

Second harmonic detection with an electric noise subtracter is described in this chapter. The noise subtracter, which is simple to build and inexpensive, automatically adjusts the subtraction ratio by using the difference between the DC photocurrents in a signal and a reference arms as a feedback signal. This method effectively reduces the signals common to both arms which includes optical feedback noise, optical fringes, and power supply pickup. In addition, the noise subtracter reduces the 2f background and reduces the dynamic range required of the lock-in amplifier by nulling the 1f intensity modulation signal. A

an ENBW of 1.25Hz for second harmonic detection at 10kHz was achieved.

CHAPTER 4 - APPLICATION OF MSXC LASER IN LIQUID DETECTION

4.1 Introduction

The near-infrared(NIR) spectral region is generally defined as a region from 0.7 μm to 2.5 μm; most of this region is covered by diode lasers developed for optical communication systems. The liquid absorption bands in the NIR are overtones and combinations of the fundamental mid-infrared (MIR) molecular vibration bands [35] and these bands are typically $\rangle$10 times weaker than the fundamental bands in the MIR region [77]. The weaker absorption is, in some sense, a blessing because the absorptance of a liquid is usually very strong for the cells of 1mm-10cm pathlength. In the NIR then, these cells can be used for many samples without extensive preparation procedures such as dilution and are much easier to work with than the 0.01cm sealed solution cells generally used for MIR work [35]. In addition, the detection system is relatively simple in the NIR region in terms of sources, detectors, and optical components such as lens and windows.

In this chapter the application of MSXC lasers in conjunction with the PCR and the PLS algorithms in detection of H_2O concentration in D_2O and in mixtures of H_2O, acetone and methanol is described. The application of the PCR and the PLS in the detection

noise sources were determined by modelling synthetic data.

4.2 Multivariate Calibration (PCR and PLS)

The PCR and the PLS algorithms [78][79] used in this work are given in Appendix B. In the PCR and the PLS algorithms, the data analysis consists of two steps. First, algorithms are calibrated for the regression coefficients by known dependent variables (known liquid concentration values in our case). The second step is to use the algorithms to give predictions for independent variables (absorbance in our case). The usual way to evaluate the performance of the models is to divide the samples with known concentrations into a calibration group and a test group. The calibration group should be chosen to span the whole sample space (concentration extent of each component in a mixture) uniformly for good predictions [80]. This can usually be done for designed experiments as in our case. The predicted values for N concentrations, $\hat{y}_i$, are compared with known values (measured by weighting), y_i, in the test group. A correlation coefficient R^2 given by

$$R^2 = 1 - \frac{\sum_{i=1}^{N} (y_i - \hat{y}_i)^2}{\sum_{i=1}^{N} (y_i - \bar{y})^2}, \qquad (28)$$

$$\text{where} \quad \bar{y} = \sum_{i=1}^{N} y_i,$$

and an rms error of prediction given by

$$RMSEP=\left[\sum_{i=1}^{N}(y_i-\hat{y}_i)^2/N\right]^{1/2}, \quad (29)$$

are generally calculated to evaluate the prediction. In some cases where the sample space can not be determined, cross-validation [76] is a more realistic evaluation method, in which one sample is left out and predicted by the calibration from all other samples at one time. After each sample is left out once, the predictions for all samples are calculated and the RMSEP from all the samples is used as an indication of accuracy for future predictions.

To understand the limiting noise in the detection scheme, we used synthetic data to simulate the noise contribution. The shapes of spectra were chosen to fit the experimental data [38] and the noises were added through random numbers with a normal distribution of a certain standard deviation. The experimental noises consisted of the noise in concentration and the noise in absorbance (deduced from measured transmission). The latter is caused by the fluctuations of laser beam, detector and electronics noises and transmission dependence on the optical system (lens, beam splitter and detectors) and is classified as the independent variable noise in the data process. From the reference channel signal fluctuations, we found that the average rms of measured absorbance fluctuations at different wavelengths is about 3.3% absorbance, i.e., the average independent variable noise is 3.3%. The noise in concentration is classified as the dependent variable noise and is the uncertainty from weighing the samples. For example, to make a 1% H_2O sample in D_2O of 20g, 0.202g H_2O has to be weighted and added. The uncertainty in readings from the balance with 0.01g sensitivity for this solution is 5% percent. In the modelling, the deviation amplitudes of added

independent and dependent noises were varied and compared with experimental data to assess noise sources and contributions. In the following section 4.3 and section 4.4, the application of the MSXC lasers in the liquid detection is described and the experimental data are processed by the PCR and the PLS algorithms.

4.3 Experimental Setup and Procedures

Fig. 4.1 shows the experimental set-up. The output of the laser was collimated by a singlet lens and then split into two beams. One beam was routed through a cuvette cell, which is made of optical glass and has a pathlength of 1cm, and then focused on the signal detector. The other beam was collected by the reference detector. The detectors were InGaAs type with a diameter of 1mm. The laser temperature was controlled by a Peltier cooler. The current of the laser was modulated by a square wave in the 1-30kHz range. Phase-sensitive detection was employed to measure the transmission through each arm, to reject ambient light, and to reduce 1/f noise. The transmission signals through the reference and the measurement arms were input to lock-in amplifiers and the outputs from the lock-in amplifiers were then recorded. The mirror was a gold coated diamond block ($250\times400\times400$ μm^3) mounted on a small drill bit [15]. The PZT was then mounted on the 5-axis stage (3 translations plus tilt and rotation), so the mirror could be placed very close(≤ 20 μm) and parallel to the back facet of the laser.

The experiments were run by a data acquisition program. After a liquid was introduced

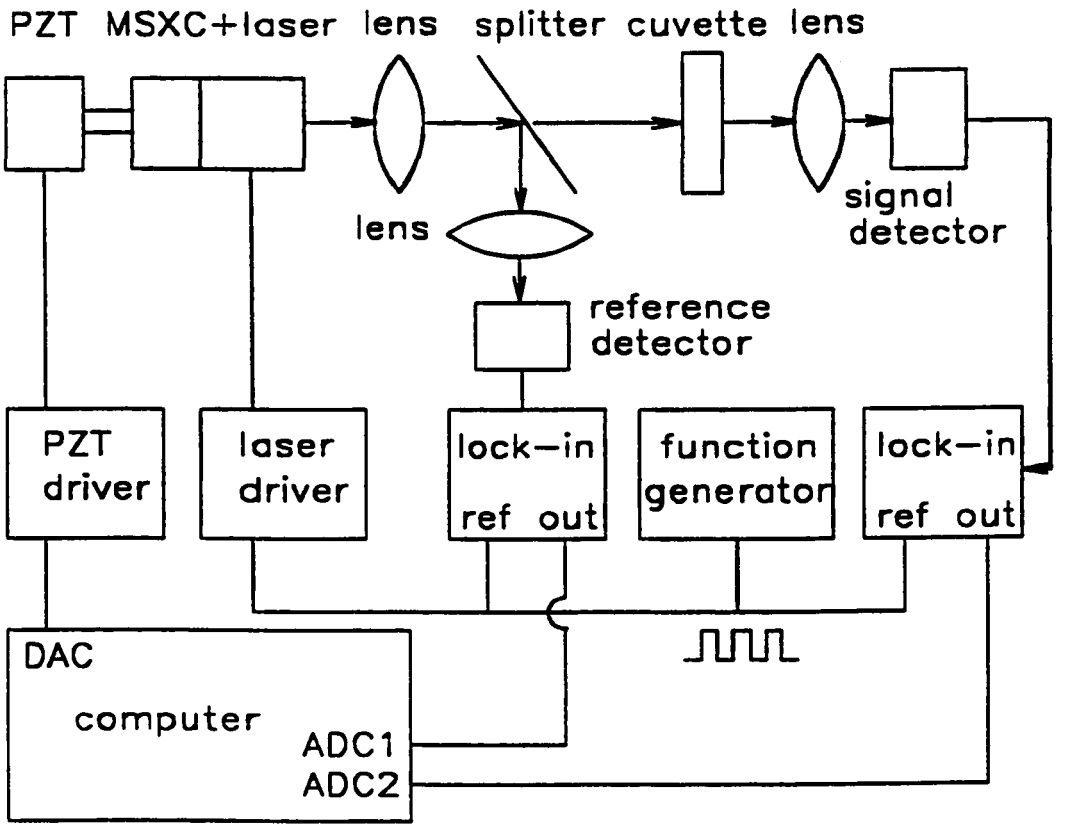

Fig. 4.1 Experimental set-up for liquid detection. The laser was modulated by a square wave at 5kHz and phase-sensitive detection was employed. The single modes were scanned by ramping the PZT voltage. The sample is in a cuvette cell of 1cm pathlength in the signal arm. The ratio of the transmission signals from the measurement arm to the reference arm are collected by the computer and processed by the PLS and the PCR algorithms.

the PZT controller with a voltage from a digital-to-analog converter(DAC). For each DAC step, the two lock-in outputs were alternately sampled 50 times by an analog-to-digital converter(ADC) and the signals were averaged to reduce the noise. The averages from the two lock-ins and the rms (root-mean-square) value of the 50 samples from the reference lock-in were stored in a file for data analysis that is discussed.

4.3.1 Spectral Output of MSXC lasers

The MSXC scheme has been developed based on the observation that while the range in wavelength is important, continuous tunability is not necessary for liquid detection. The laser was an InGaAsP/InP strained-layer multiple-quantum-well ridge-waveguide laser with a length of 250 μm [85], lasing at 1.40 μm where water has an O-H stretch first overtone absorption peak [35]. Fig. 4.2 shows an example of the spectral output of the 1.40 μm MSXC laser at a current of 55mA and temperature of 22°C. Eighteen distinct modes with an average side mode suppression ratio (SMSR) of 1.3% are obtained as the position of the mirror is changed by $\lambda/2$. The difference in wavelength of the first mode to the last mode is 72nm. When the mirror is moved lasing switches typically from the lasing mode to a mode spaced 4 free-running laser modes away, or switches to a mode 3 free-running modes away and then quickly switches to the fourth mode. In 2 or 3 regions, the laser operates briefly multimode operation and then switches to the fourth mode away. The regions of single mode operation as shown in Fig. 4.2 can be determined by analyzing the noise power as discussed in the next section.

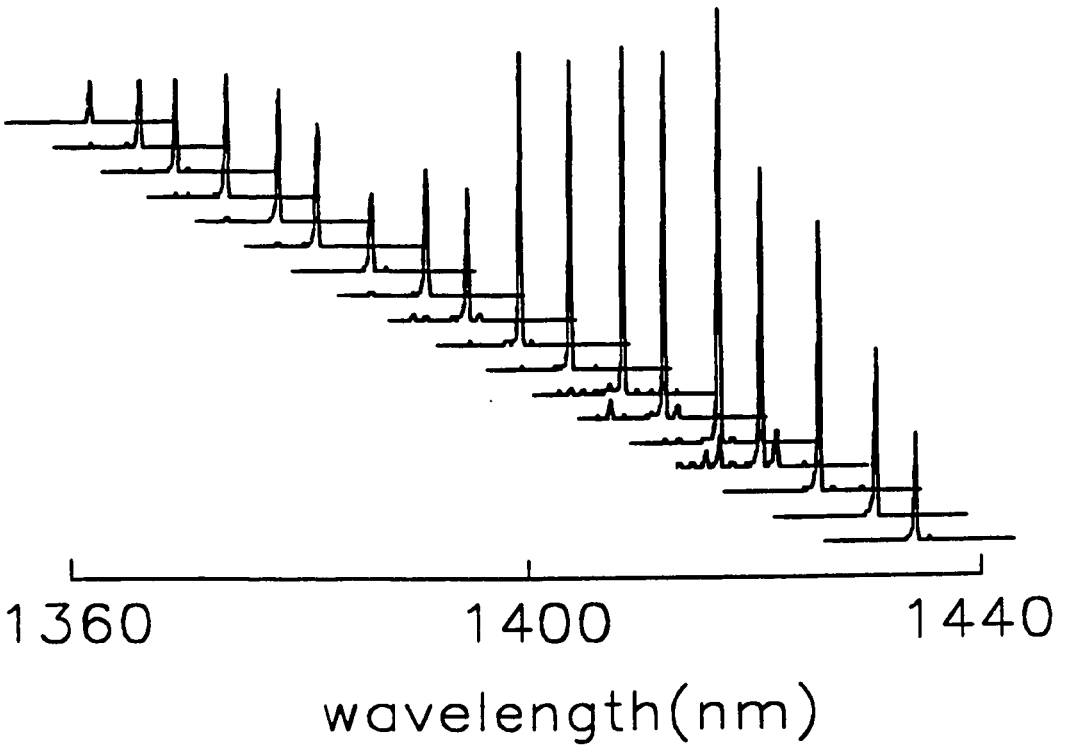

Fig. 4.2 The spectral output for the MSXC laser at I=55mA and T=22°C as the distance of the mirror behind the laser is scanned. A total of 18 distinct modes was obtained. The difference in wavelength from the first mode to the last mode is 72nm.

4.3.2 Determination of Single-Mode Operation Regions

The MSXC laser is essentially a monochromatic source. The measurement of the absorption of liquids at different wavelengths of the diode laser can be done without any additional dispersive elements for wavelength selection. This is one advantage offered by the diode laser, but the questions are how to know that the diode laser is operating on a single mode region and which single mode is it. After comparing several methods, including ways to dither the PZT voltage or diode current and then measure signals at the first harmonic (1f) or the second harmonic (2f) of the dither frequency, we found the best results were obtained by simply measuring the rms values of the reference beam. Fig. 4.3 shows typical signals from the reference channel as the mirror is scanned over $\lambda/2$. The upper trace is the average power of 50 samples and the lower trace is the rms values ($\times 100$) of the samples for each mirror step. Near the position of the mirror where the laser switches the mode, the rms value of the power has a spike because the competition between the modes gives a large variation of the power of the laser beam. Single mode regions have a small and flat rms value. The mode pattern is repeated if the mirror scans across the same range, and if the mirror moves a further distance of $\lambda/2$ the pattern will repeat but with a few more spikes because there are 2-3 more modes in a one $\lambda/2$ period. A program was written to determine the single mode regions by first searching for peaks plus some other criteria such as the amplitude of the rms values and the distance between the peaks. The middle between the peaks was taken as a single mode region. It can be seen in the upper trace

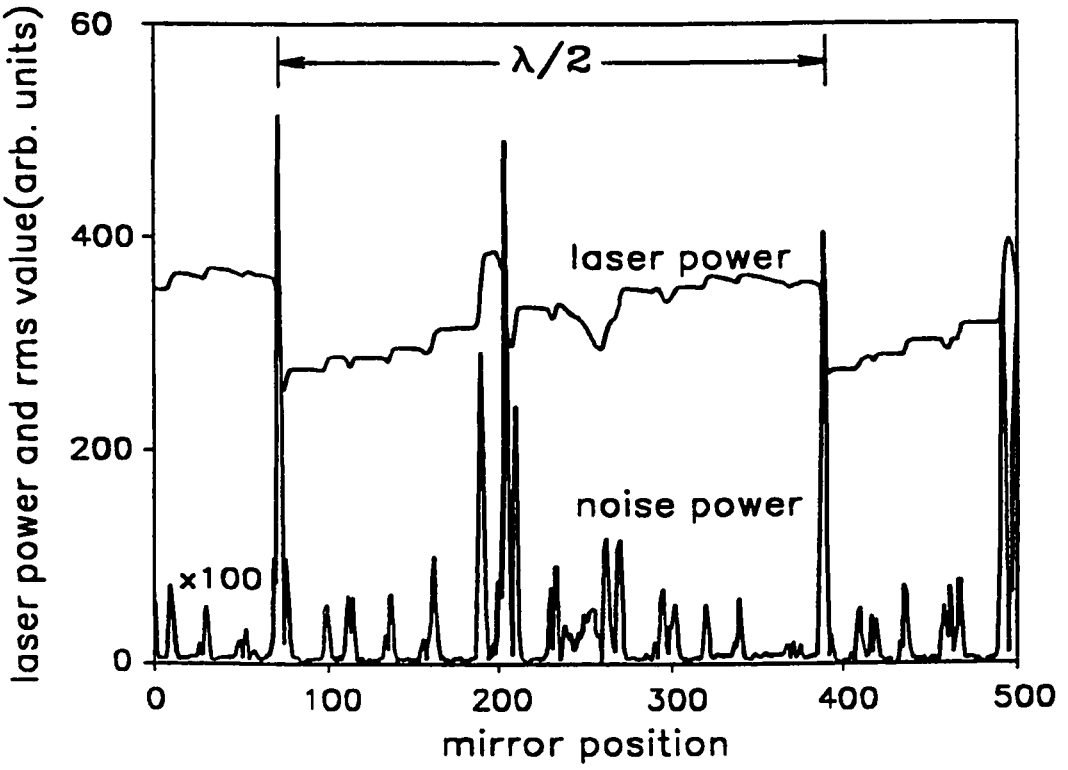

Fig. 4.3 The laser power and rms values versus the mirror position. The spikes on the rms values are caused by the competition of the laser power between the laser modes, and mark the position where the laser mode hops. One mode period($\lambda/2$) is shown from channel 80 to channel 400. The single mode regions are identified by processing the rms spectrum.

i.e., in the regions between the two spikes in the bottom trace, because the feedback level from the MSXC changes when the mirror moves. Thus it is necessary to use a reference arm and a signal arm. The ratio of the power in the signal arm to the power in the reference arm depends on the absorption and not the laser power. In addition, some of the noise of the laser can be divided out in the double beam configuration. It should be noted that the wavelength of each mode is fixed for a constant current and temperature and that the shift in wavelength caused by the variation of feedback from the MSXC is less than 0.5% of the spacing between modes ($\sim$ 1nm) of the laser. The absolute position of wavelength for each mode can be measured by a monochromator, but it is not necessary to know for liquid detection as long as the calibration sets and the measurements are done for the same current and temperature of the laser.

4.4 Results and Discussion

Samples of H_2O in D_2O and samples of mixtures of H_2O, acetone and methanol were made by mixing pure substances. the purity of D_2O (MSD Isotopes) was 99.9%, acetone (Caledon Laboratories Ltd.) was 99.5% and methanol (Caledon Laboratories Ltd.) was 99.8%, the H_2O was from three-column purified filter system (Barnstead). The pure substances were weighted according to designed weights by an electronic balance with a sensitivity of 0.01g and mixed. The weighted concentration values were used as both the calibration values and the test values.

To show that the spectral coverage of the MSXC laser is sufficient for selective detection of liquids, for each single mode, the transmission (T) from the sample arm was recorded for a blank cuvette cell, a cell with pure acetone, a cell with pure methanol, and a cell with a solution of 25% H_2O+75% D_2O(by weight). The absorbance (log(1/T)) for the three liquids at 17 different wavelengths is shown in Fig. 4.4. The data from the blank cell were used as the intensity reference. The values are consistent with the spectrum obtained by FT-IR spectrometer[35]. The H_2O was diluted by D_2O because the absorption peak is too strong to measure for a 1cm pathlength cell. Fig. 4.4 clearly shows that the absorptions of the liquids are sufficiently different over the 72nm wavelength range obtained with the MSXC laser to consider detection of the concentration of water in the other liquids. This will be further seen in the following sections.

4.4.2 H_2O Concentration in D_2O

H_2O has an O-H stretch overtone absorption peak around 1.4 μm, the overtone absorption peak of D_2O is shifted to 2 μm [35], so D_2O can be used as a solvent for many other liquids in this spectral region. 15 samples with H_2O concentration in D_2O ranging from 0-7% by weight were divided into two groups, 8 samples were used for calibration in the PCR and the PLS. Fig. 4.5(a) shows the H_2O concentration predicted by the diode laser with the PCR for N=7 test samples after two factors, plotted versus the weighted

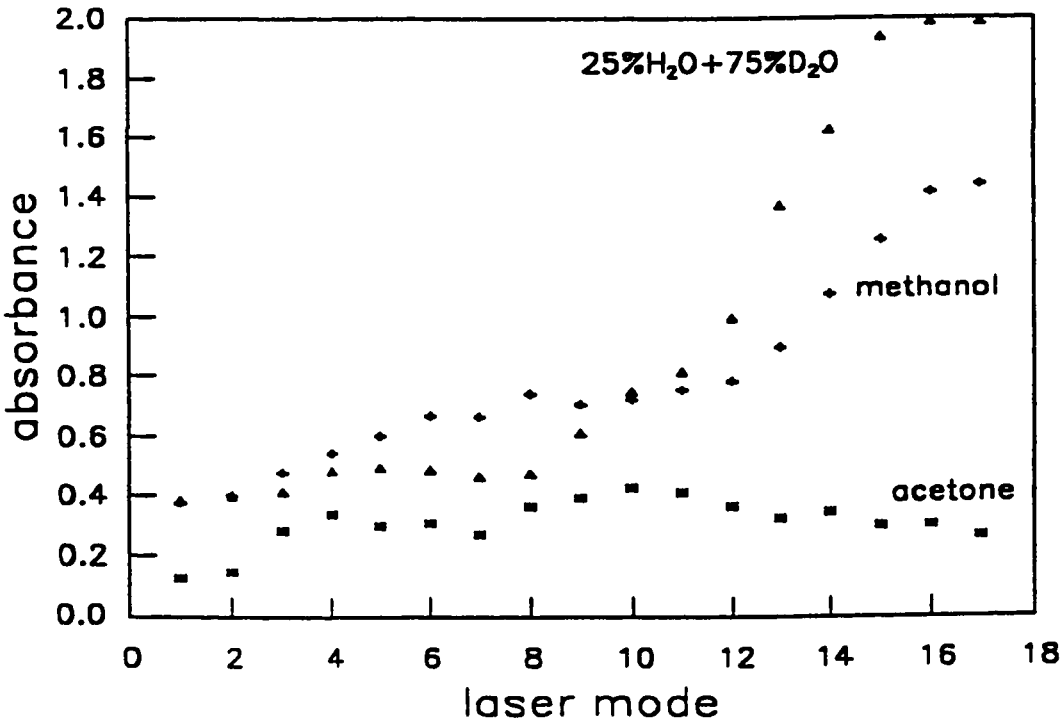

Fig. 4.4 The spectra of acetone, methanol, and a mixture of H_2O and D_2O over 17 single laser modes. H_2O was diluted because the absorptance at 1.45μm peak is too strong for the 1cm cell. The contrast shows that the MSXC laser provides a wide enough spectral coverage for liquid detection.

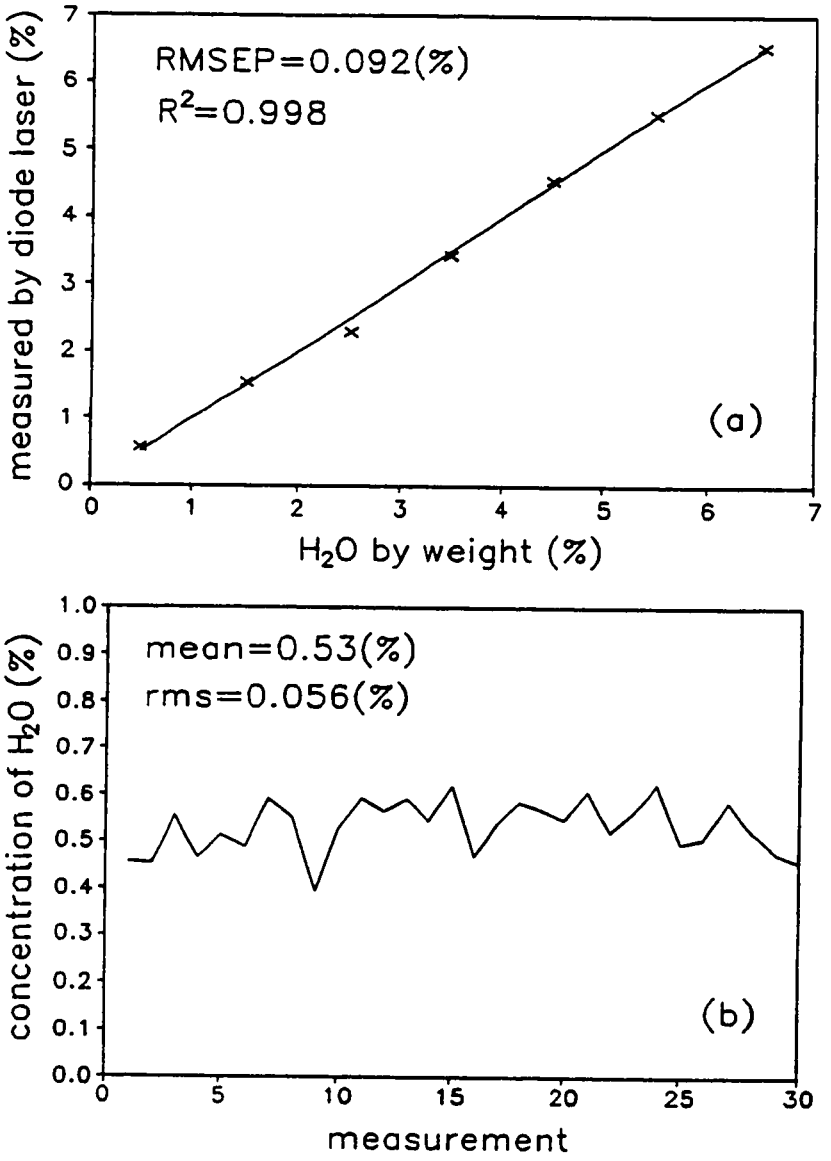

Fig 4.5 (a): The prediction of H_2O concentration by diode laser spectroscopy versus the true values (weighted values) by the PCR. The straight line is the ideal prediction with a slope of unity. The prediction from the diode laser has an R^2 of 0.998 and an RMSEP of 0.092%. (b): 30 repeated measurements for 0.5% H_2O concentration with the mean value of 0.53% and rms value of 0.056%. The rms value shows the accuracy of the detection scheme.

values. An R^2=0.998 and an RMSEP=0.092 percentage points were obtained by the PCR. The PLS gave an R^2=0.995 and an RMSEP=0.14 percentage points for the same data after two factors. Fig. 4.5(b) shows that the 0.5% point was measured 30 times. The absorbance data were fed into the PCR to give 30 predictions. The mean value was 0.53% and the rms value was 0.056%. This result implies that the method is sensitive to detect 0.1% concentration difference of H_2O in D_2O.

Because the sum of H_2O and D_2O was equal to 1, the system should be a one factor system, which is in agreement with the steep drop of the RMSEP after one factor. But the minimal RMSEP was obtained after two factors. It is believed that the additional factor was mainly caused by the wavelength dependence of the lens, the beam splitter and the detectors [38]. Fig. 4.5(a) and Fig. 4.5(b) reflect the precision of predictions for different concentrations (RMSEP) and the accuracy of the prediction for 0.5% concentration. They respond differently to the independent and the dependent noise sources. A modelling of synthetic H_2O in D_2O data shows that the dependent variable errors are the dominant noise source for the experimental RMSEP. They contribute to the RMSEP through both the calibration group and the test group with the latter being significant because y_i is not an averaged value and is used as true value to calculate the RMSEP. The independent variable noises are accounted for in the accuracy of the predictions. The modelling showed that the contribution of the independent variable noises to RMSEP was minimal compared to the dependent variable noises because the random noises in the absorbance could be reduced by averaging in multivariate calibration. The reduction was influenced by the spectral contrast

between the H_2O spectrum and the background signals.

4.4.3 Mixtures of H_2O, Acetone and Methanol

50 samples of H_2O, acetone and methanol mixture were made by weighting pure substances, the concentrations of H_2O, acetone and methanol range 2-10%, 0-98% and 0-90%, respectively, the sum percentage of the three substance was equal to 100. They were divided into 30 calibration samples which covered the boundary concentration values of the pure substances and 20 test samples. Fig. 4.6(a), (b) and (c) show that predictions by the PCR versus the weighted values, the RMSEP for H_2O, acetone and methanol for 20 test samples were 0.49%, 1.28% and 1.45% respectively, which implies that the method can give the predictions within ~ 1.5% for each component in the mixture. Fig. 4.7 shows that the RMSEP versus factors for three component predictions. It can be seen that RMSEP has a sharp drop after 2 factors which is agreement with a 2 factor system (three component system with the sum percentage of 1). The minimal RMSEP is achieved after 5 factors and the additional factors after 2 slightly reduce the RMSEP. The 95% confidence intervals of the RMSEP using a χ^2-test [81] from factor 2 to factor 10 are [0.09, 0.25], [0.43, 1.23] and [0.31, 0.88] for H_2O, methanol and acetone, respectively, so 2 to 5 factors are acceptable factor numbers for this system. The additional factors are attributed to the noises and the wavelength dependence of the system. The modelling showed that the dominant noise source for RMSEP in this case is the dependent variables noise as discussed in section 4.2. If there are no dependent variable noise, for a 3.3% independent variable noise, the

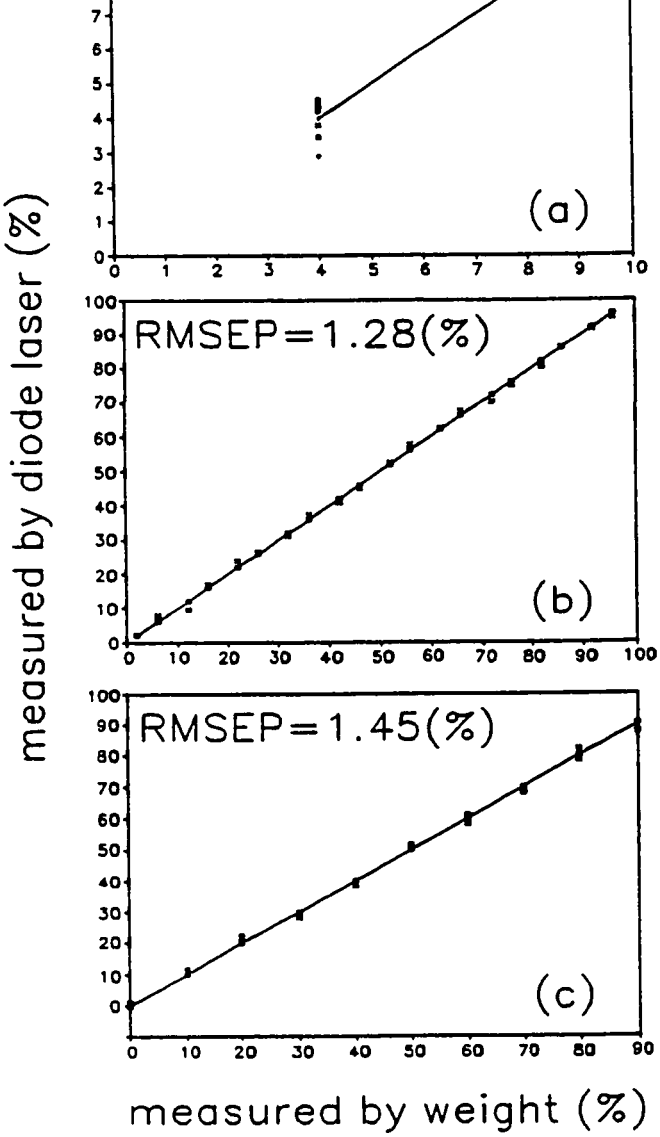

Fig. 4.6 The predictions of H_2O, acetone and methanol concentration in 20 test samples versus the true values (weighted values) in the mixtures of H_2O, acetone and methanol by the PCR. (a): H_2O predictions with a R^2=0.941 and an RMSEP=0.49%, (b): acetone predictions with a R^2=0.998 and an RMSEP=1.28% and (c): methanol predictions with a R^2=0.998 and an RMSEP=1.45%. 5 factors are used to obtain these predictions. The predictions shows the detection capability of the scheme in a mixture. The precision of the predictions are mainly limited by the weighting errors as discussed in the text.

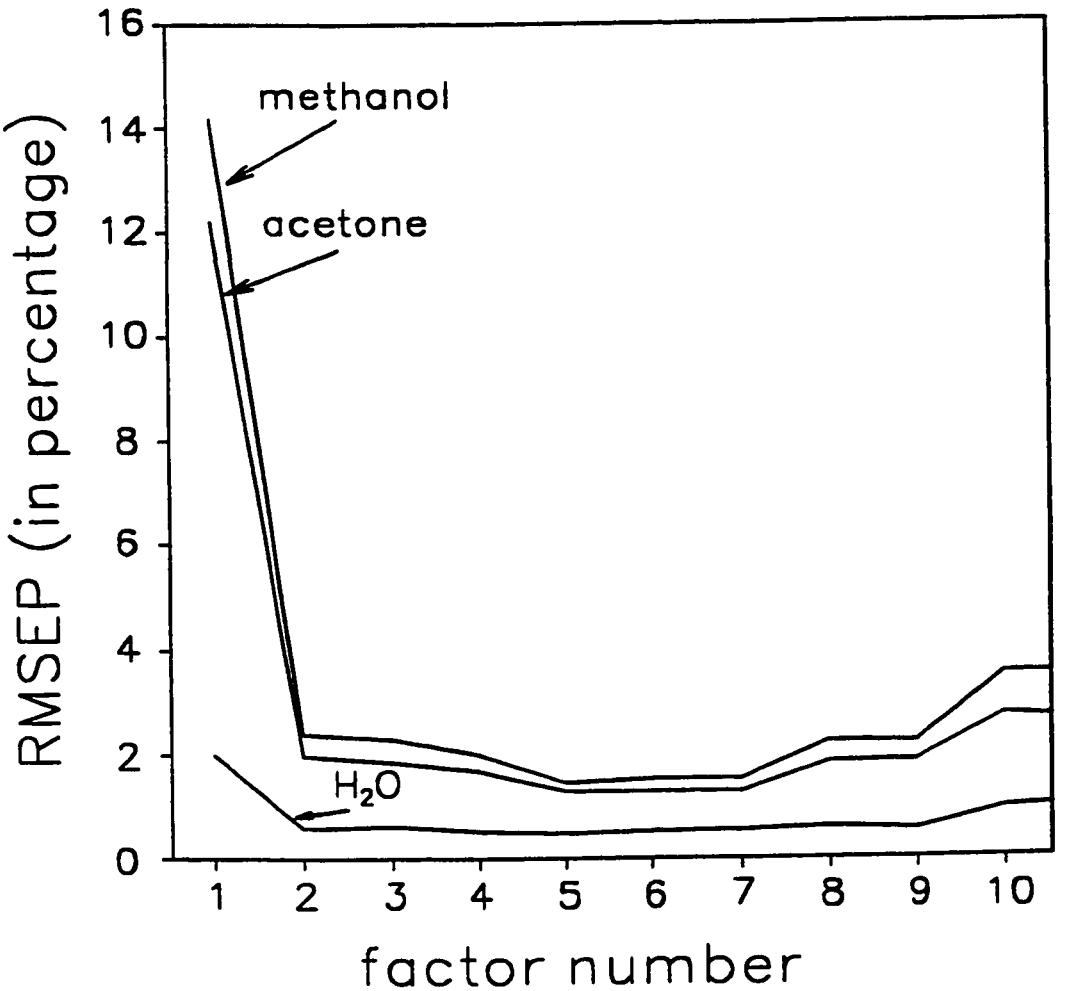

Fig. 4.7 The effect of number of PCR factors on the RMSEP for H_2O, acetone and methanol. The steep drop after two factors shows that the system is a two factor system (three component with sum of percentages equal to 1). The minimal RMSEP is achieved after 5 factors. The additional factors are attributed to the effect of wavelength dependence and noises in detection system.

Fig. 4.8 shows the capability of the detection of outliers in this scheme. Here outlier means a sample that does not belong to the calibration group in that the absorption is beyond what was expected. 6 samples of H_2O in D_2O (with no acetone or methanol) with concentrations ranging from 3% to 33% were made as outliers. Residues for the 20 test samples that were in the range of calibration together with residues for the outliers are plotted against wavelength. From the structure of the residues it can be seen clearly that the spectra from the outliers and the blank cell do not belong to the calibration cluster. Outlier warning can be given to these groups to avoid mistaking them as mixtures of H_2O, acetone and methanol. The PLS could not successfully be applied in the three mixture case because there is a correlation between acetone and methanol concentrations in the designed mixture. The influence of the correlation was modeled in the synthetic data and it was found that erroneous predictions were caused because the PLS algorithm could mistakenly use spectral information from one component in the regression for another component due to the correlation. Chung et. al [82] has pointed out the correlation effect in the PLS. One should be careful when using the PLS algorithm for a mixture in which the concentrations of two components may be correlated with each other.

4.5 Summary

A scheme of liquid detection by the MSXC diode lasers with multivariate calibration

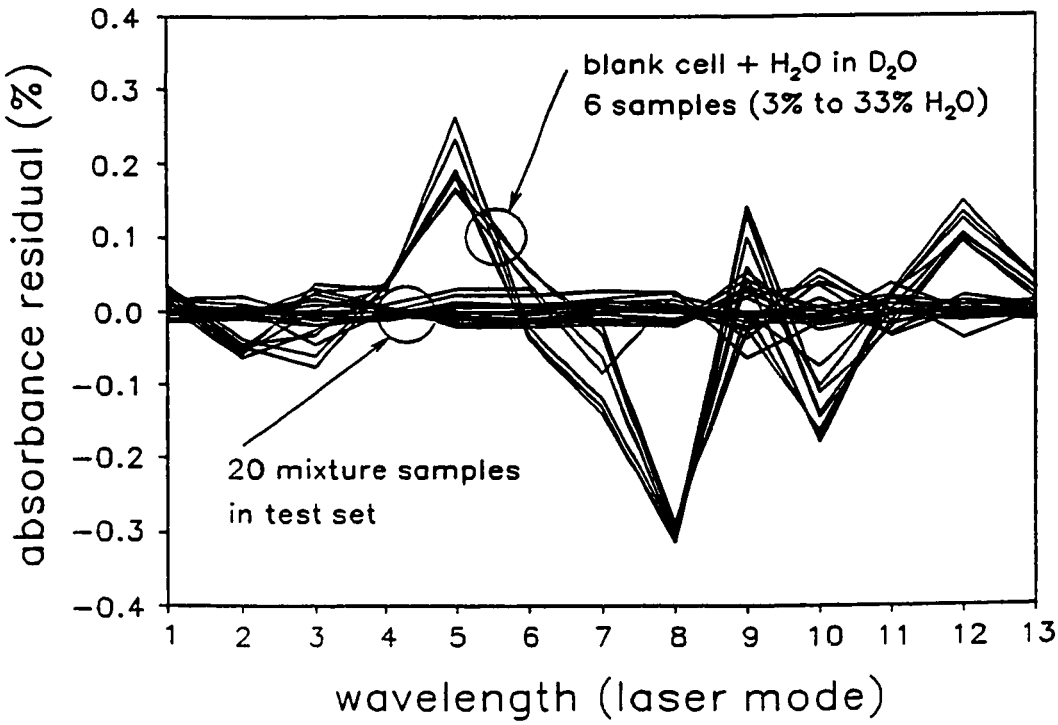

Fig 4.8 The absorbance residuals versus wavelength after 5 factors for 20 test samples and the outlier. The outlier consist of 6 H_2O in D_2O samples with 3-33% concentrations and a measured absorbance from a blank cell. The structure and the amplitude of the residuals from the outlier clearly show that they are not belong to the cluster of the calibration set. The outlier warnings can be given to avoid mistaking them as the mixture of H_2O, acetone and methanol.

has been presented. The scheme may be used to make compact and low cost liquid sensors for the applications such as liquid detection and identification in industrial process control. The scheme can provide adequate predictions for H_2O concentration in other liquids and for a three component mixture. The factor analysis and the outlier detection can be used to give more reliable predictions for mixtures. It is found that the RMSEP is 0.1% for H_2O in D_2O, and about 1.5% for each component in the mixture of H_2O, acetone and methanol. The result of repeated measurements of 0.5% H_2O in D_2O shows that the method has a sensitivity to detect 0.1% difference. The modelling of a synthetic data shows that the uncertainty in the concentration due to limited precision in weighing of samples is the dominant noise source in the measurement.

CHAPTER 5 - DESIGN OF QUANTUM WELL DIODE LASERS WITH BROAD GAIN PROFILE

5.1 Introduction

In the discussion of Chapter 2, the gain profile was approximated by a parabolic function and the maximum tunable range was given by the difference of the extremes of wavelength away from the gain centre where the dip of reduced loss intersected the gain curve. The magnitude of the reduced loss is determined by the fraction of the reflected light that couples into the active region. Besides the coupling efficiencies, the tunable range is intrinsically decided by the shape of the gain profile of a semiconductor diode laser. A broad and flat gain profile will permit operation on wavelengths far from the gain centre. Based on this consideration, work to design a semiconductor diode laser with a broad and flat gain profile for spectroscopic application was initiated. The laser with a potential to tune broadly is not only very useful in detecting the broad spectral features of liquids, but also is desirable in tunable lasers for gaseous state spectroscopy. In the first part of this chapter, the considerations in design of a broad gain profile diode laser are discussed and some simulated results of important properties of a diode laser are presented. In the second part of this chapter, the experiment results are reported and discussed.

With the development of growth techniques such as MBE and MOCVD in the past 15 years quantum wells lasers have become a reality and gained increasing popularity. Besides many advantages such as high efficiency, low current threshold, temperature dependence and frequency response, quantum well provide a means to manipulate the bandgap by choosing the thickness and composition of the wells. Introducing strain to quantum wells was originally proposed in 1986 [83]. It has since become a very useful means to engineer the band structure and provide improved performance of lasers [84].

The main concern of diode lasers applied in spectroscopy is the wavelength coverage and the band-structure engineering available in quantum well lasers provides a tool to design a diode laser which covers a wavelength region of spectroscopic interest. There are many design parameters to be specified in the modelling a strained quantum well laser and includes the number of quantum wells, thicknesses, strain, composition of quantum wells and barrier layers, geometrical structure, composition and doping level of the confinement regions, and the structure of the ridge waveguide.

The modelling was done with the LASTIP package [85] at the Institute for Microstructure Science (IMS), National Research Council (NRC). The program permits users to choose all the parameters mentioned above and simulates many lasing characteristics. The main considerations for design of this laser were the following. (a): Wavelength centre

at 1.4 μm where there are many very strong absorption water vapour lines. The potential application is to detect humidity fluctuation in meteorology [86]. (b): A broad and flat gain profile. It is desired that a tunable range from 1350 to 1450nm can be achieved by means of the external feedback discussed in Chapter 2. Liquid H_2O has a absorption peak from 1360nm to 1470nm [35] and the laser can be used to detect H_2O concentration in organic solvents which is a common quantity of interest to know in many industrial processes. (c): The laser is desired to lase for a length of 250 μm or shorter. A short length laser must be pumped hard to achieve threshold and then more energy levels are populated by the carrier and the gain profile tends to become flat.

It should be noted that some features of a diode laser are desired for both telecommunication and spectroscopy such as low threshold, high efficiency and output power, and symmetry far-field, but high chirp is desired for spectroscopic application. High speed modulation is not considered important for the design.

Fig. 5.1 shows the structure of the InGaAsP/InP strained multiple quantum well laser at 1.4 μm with a broad gain peak. The novelty of the laser is that there are two different types of quantum wells in the structure. One type of well has a thickness of 30Å and the other has a thickness of 60Å. The thickness, the composition and the strain level are chosen such that the centre of the gain profile is at 1.4 μm and is broad and flat where the gain contributed from the two quantum wells overlap. Fig. 5.2(a) and (b) show the calculated spontaneous emission and the gain curves versus the pumping current from 15mA to 90mA.

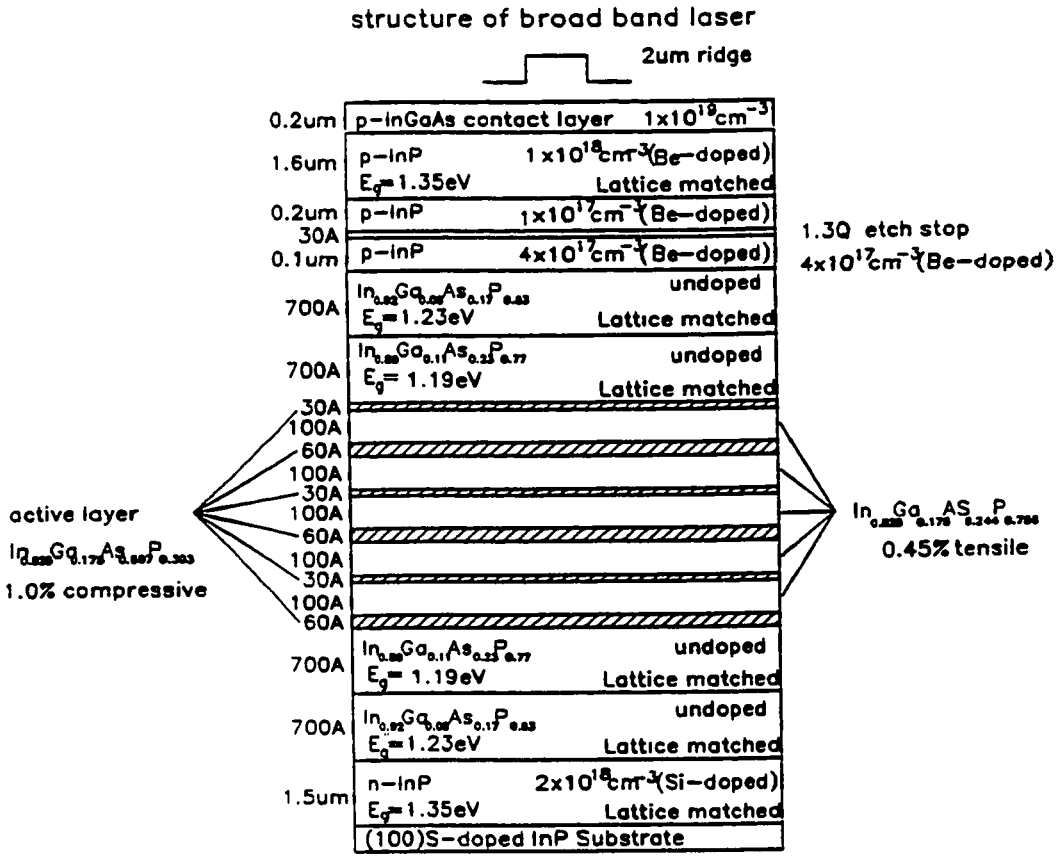

Fig. 5.1 The designed structure of the InGaAsP/InP strained multiple quantum well lasers at 1.4 μm with a broad gain. The laser has two different types of quantum wells in the structure to achieve a broad and flat gain curve, one has a thickness of 30Å and another has a thickness of 60Å.

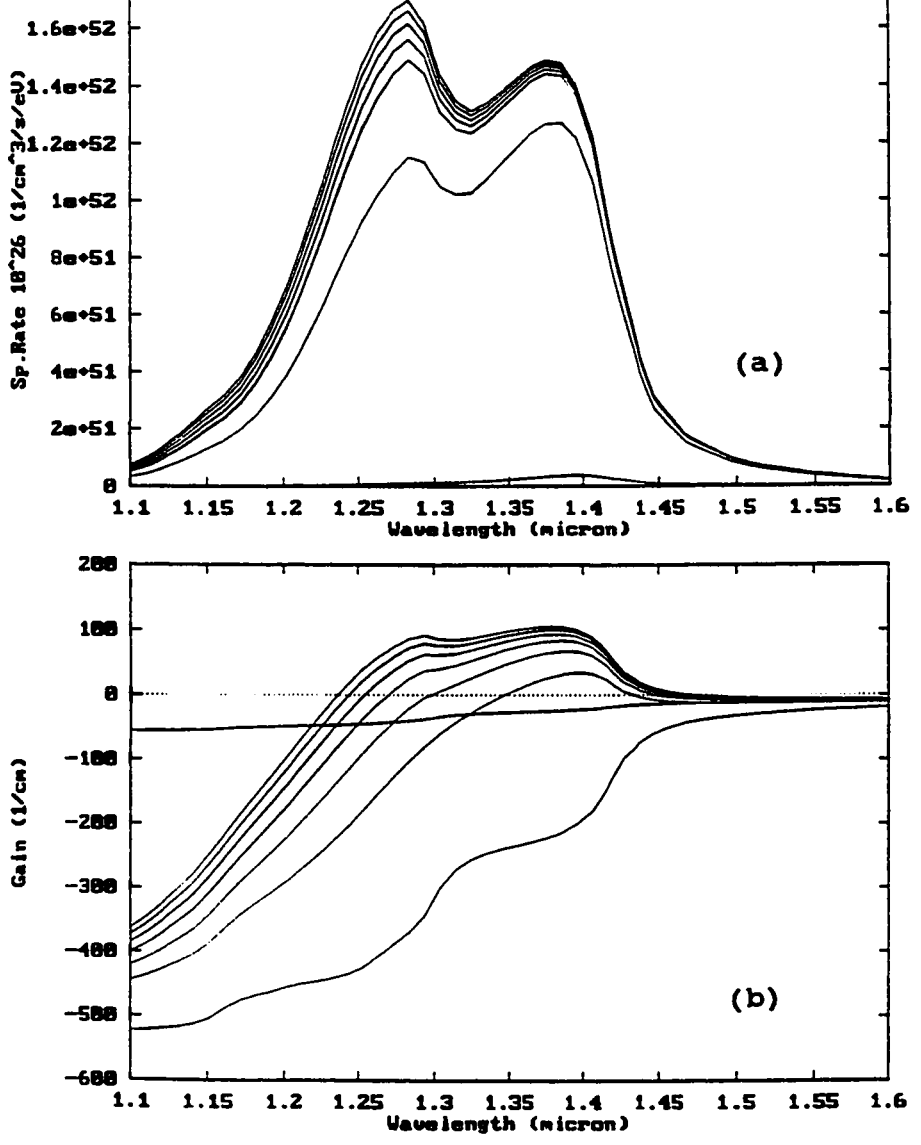

Fig. 5.2 The simulated spontaneous emission (a) and the gain curves (b) versus the pumping current from 15mA to 90mA for a laser with a length of 100μm. The two peaks at 1.27μm and 1.39μm in the spontaneous are the contribution from two the types of quantum wells. The gain curve is flat under a sufficient pumping and is more than two time broader than a simulated one with identical wells.

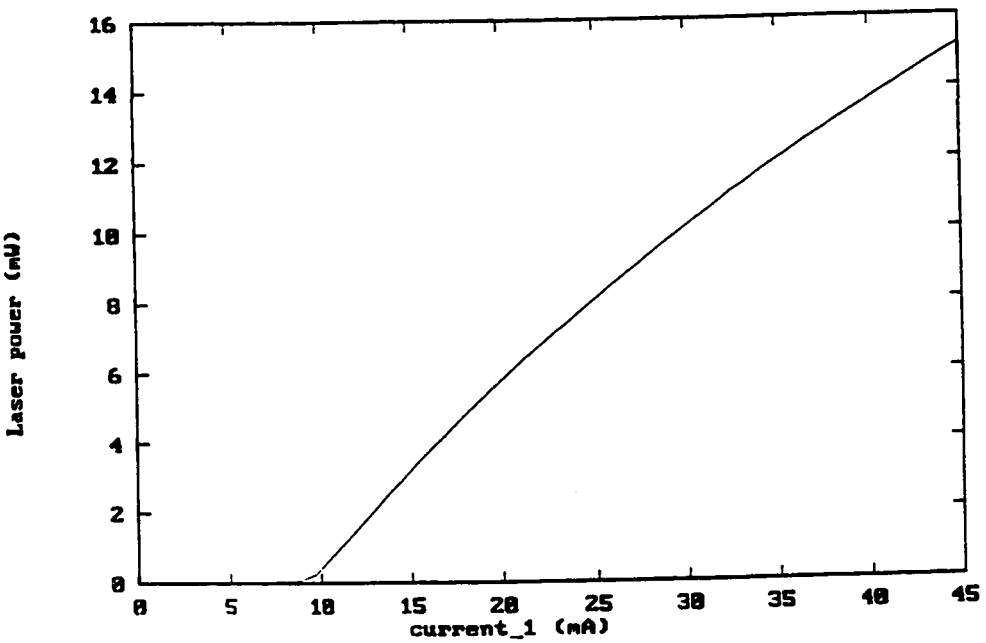

Fig. 5.3 The simulated L-I curve for a laser with a length of 250μm. The structure is predicted to reach the threshold for lasing at 10mA under the assumption of quality material and processing.

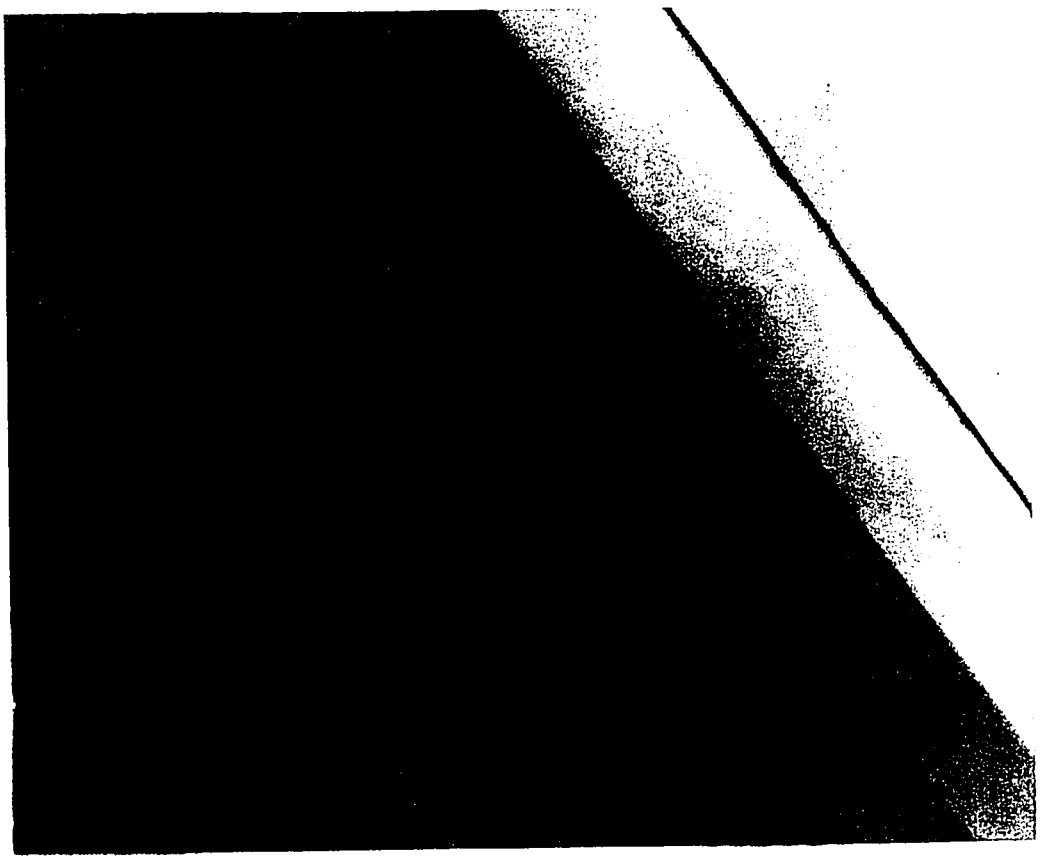

Fig. 5.4 TME photograph of the laser structure. The image shows that all layers are quite uniform and the interface between the various quaternary compositions are sharp. The measured thicknesses of two types of quantum wells are 38Å and 68Å.

The curves are shown for a laser with a length of 100 μm. The spontaneous emission curve shows the contribution from two types of quantum wells which peak at 1.27 μm and 1.39 μm, respectively. The short length is used to show the gain curve under high current pumping. The gain curve will be pinned to the Fermi level when the lasing action starts. For comparison, a simulation has been done on a multiple quantum well laser at 1.39 μm with 5 identical 38Å wells [87] under the same material parameters. The gain curve of the laser with two different quantum wells is more than two times broader than the one with identical wells. One percent compressive strain has been chosen because of its high efficiency shown by the simulation and examples in the literature [85]. The thickness of the active layer of 270Å exceeds the critical thickness for strain relaxation [88]. The barrier layers are then chosen to have 0.45% tensile strain to compensate the total strain.

Fig. 5.3 shows the simulated L-I curve for a laser with a length of 250 μm. The structure is predicted to reach the threshold for lasing at 10mA at room temperature under the assumption of a quality material and processing. There were many other simulated characterizations such as I-V curve, peak gain versus current near-field and far-field distribution, carrier concentration across the layers and bandgap diagram under different bias current which were examined.

5.3 Performance of Diode Lasers with Broad Gain Profile

The laser was grown by gas source molecular beam epitaxy at McMaster University.

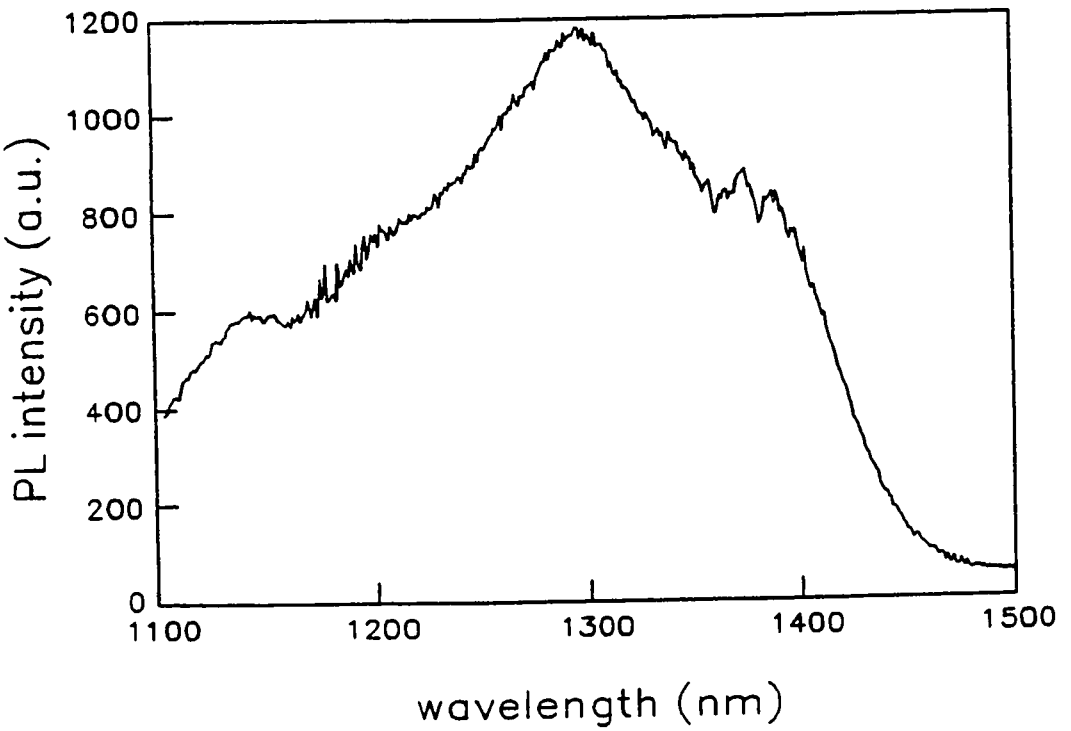

Fig. 5.5 The photoluminescence spectrum from the edge-pumped PL shows a broad peak from 1200nm to 1400nm. The PL spectrum is generally in agreement to the simulated spontaneous emission with the two peaks slightly shifted to longer wavelength due to the fact that quantum wells are thicker than the designed ones.

The broad area devices were processed at the NRC and ridge waveguide (2 μm to 5 μm) lasers were processed at McMaster University. Fig. 5.4 is the transmission electron micrography (TEM) taken at NRC [89]. The measurements from TEM showed that the thickness of the two type of quantum wells were actually 38Å and 68Å, and the thickness of the barrier layer was 97Å, which imply the gain will slightly shift to longer wavelength than the designed one. The TEM image reveals that all layers are quite uniform and the interface between the various quaternary compositions are sharp and that there are no visible defects.

Fig. 5.5 is a plot of the edge-pumped photoluminescence [90], and shows a broad PL spectrum from 1200nm to 1400nm. Although it is difficult to compare numerically, the PL spectrum is generally in agreement to the spontaneous emission shown in Fig. 5.2(a) with the two peaks slightly shifted to longer wavelength due to fact that the quantum wells are thicker than the designed ones. Fig. 5.6(a) shows the centre wavelength and the density of threshold current versus cavity length for broad area lasers. Fig. 5.6(b) shows the plot of $1/\eta$ versus the cavity length of lasers [87]. The difference in operating wavelength is 90nm for lengths from 200 μm to 1500 μm, which is about 2.5 times larger than the observed difference for a laser with all quantum wells of nominally the same thickness (i.e., a typical laser) [91]. The loss and internal efficiency deduced were 7.5cm^{-1} and 37%, respectively, which are among the best device performance of quantum well lasers in this region. The ridge waveguide lasers were fabricated at McMaster University [92]. For lasers with 2 μm ridge and 250 μm length, the typical threshold current was about 30mA. Preliminary

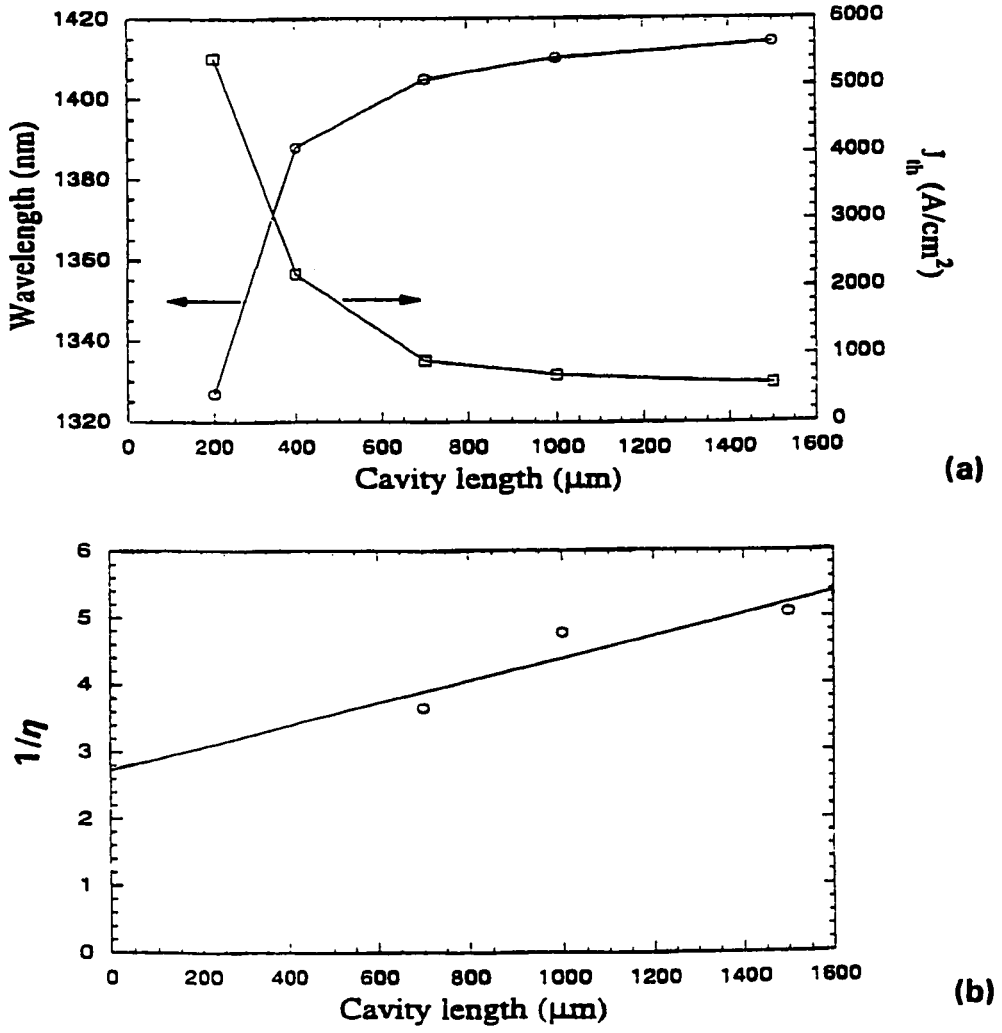

Fig. 5.6 (a): Threshold current density and centre wavelength as a function of cavity length for broad area lasers. The wavelength shift is 90 nm for the length from 200 μm to 1500 μm, which is significant broader than a typical laser with one type of quantum well. (b): Inverse efficiency as function of cavity length for broad area lasers. The loss and internal efficiency were deduced to be 7.5 cm^{-1} and 37 %.

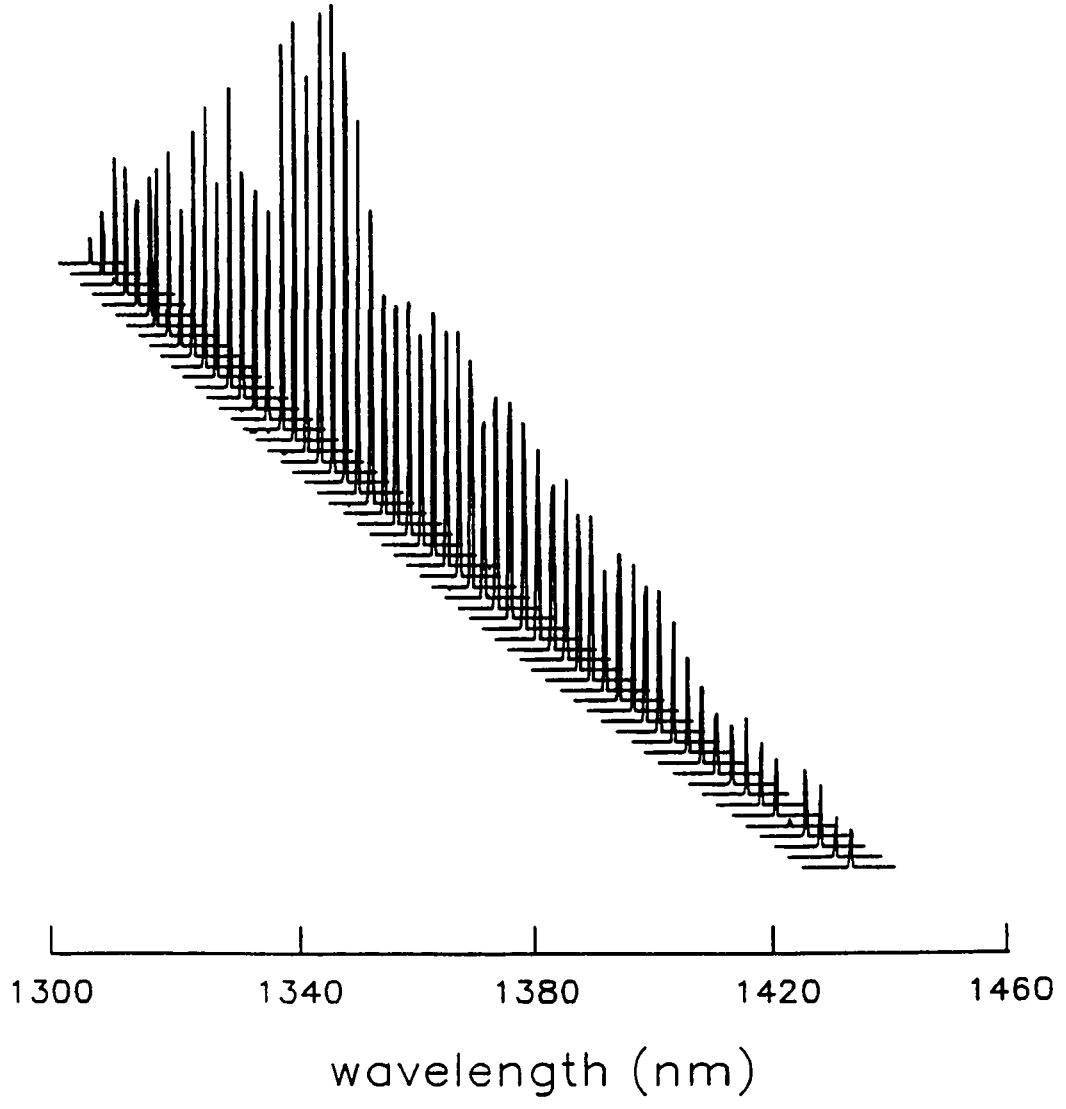

Fig. 5.7 The spectral output for a broad gain peak laser in a GEC scheme at I = 90 mA and T = 22°C, as shown for every other mode. The laser has a length of 250 μm, a 2 μm ridge, and is not antireflection coated. The wavelength is tuned by rotating the grating. The difference in wavelength from the first mode to the laser mode is 118 nm, which is about 3 times wider than results from a conventional diode laser.

results showed that the lasers can be tuned very broadly by an external feedback. Fig. 5.7 shows the output of a broad gain peak laser in the GEC scheme. The laser was not antireflection coated and was operated at 90mA and 22°C. The wavelength of the the laser was tuned by rotating the grating. The span of wavelength from the first mode to the last mode is 118nm. This tunable range is about 3 times wider than the results from the conventional diode lasers with identical quantum wells. Further characterization and application in spectroscopy of the ridge waveguide structure lasers are being actively pursued at McMaster University.

CHAPTER 6 - CONCLUSION

6.1 Summary of Thesis

This thesis has described a few schemes of tunable diode lasers and their application in trace species detections. The scope of this work involved design of a broadly tunable diode laser, construction of external cavity diode lasers, and high sensitive gas detection and liquid detection. The operation and comparison of SXC, MSXC and GEC lasers was presented in Chapter 2, and an empirical model based on gain profile and reduced loss due to external cavity feedback was used to explain the tuning mechanism of SXC, MSXC and GEC. In Chapter 3, highly sensitive trace gas detection was studied by means of modulation and subtraction. An analysis for the modulation spectroscopy of a diode laser based on the concept that the light intensity is directly modulated by the injection current together with an experimental confirmation was presented. A subtraction scheme to reduce the noise for second harmonic (2f) detection was reported and a noise level equivalent to a line centre absorption of 1.6×10^{-6} was achieved with an ENBW of 1.25Hz for 2f detection at 10kHz. In Chapter 4, a MSXC laser with spectral coverage up to 72nm was used in a scheme for detection of liquids in conjunction with the PCR and the PLS algorithms. Detection of H_2O concentration in D_2O with a sensitivity of $\sim 0.1\%$ and in a three component

mixture of H_2O, acetone and methanol with a sensitivity of $\sim 1.5\%$ were demonstrated. The properties of the PCR and the PLS were studied in terms of the optimizing factor and the detection of outliers. Finally, the design of a strained multiple quantum well laser consisting of two different type wells with a broad gain profile was described. Preliminary measurements about the characterization of the broad gain peak laser were reported.

6.2 Suggestions for Further Research and Development

Much of the work reported in this thesis is the initial step to achieve better performance from tunable diode lasers and to find new applications of tunable diode lasers in trace species detection. These are many leads to future research; the followings are considered to be interesting and natural extensions.

An empirical description with a parabolic gain profile was used in Chapter 2 to explain the tuning mechanism of a MSXC laser. An analysis by using a Fabry-Pérot model [93] may provide a better understanding and provide a calculation of the intensity in each mode. It is also desirable that further modelling include a mechanism to explain that the gain peak becomes broader for a higher current pumping.

In Chapter 3, the analysis and experiments for the modulation spectroscopy of a diode laser based on the concept that the light intensity rather than the electric field is directly modulated by the injection current was presented. It is interesting to know in detail

with one recent work [94] which discussed a lineshape in FM spectroscopy based on a modulated electric field.

A theoretical study in the design of a diode laser with a broad gain peak for spectroscopic application may be a very rich and interesting area to pursue. Band structure engineering in strained quantum well lasers has been proved to be vital in the realization of high performance diode lasers for telecommunication. It is relatively new to design a broad gain peak laser for spectroscopy. Recently one work [95] (published after the laser with the broad gain peak was grown at McMaster) presented a theoretical calculation about a possible quantum well laser with dual-wavelength operation by using asymmetrical quantum wells.

Use of MSXC lasers in conjunction with multivariate calibration is a new approach to detection where the spectral features are broad. It may be possible to replace Fourier-Transform spectrometers in many industrial applications such as determining protein concentration in wheat by a compact, cheap MSXC laser based sensor. Another possible application of a MSXC laser is to detect ice on airplane wings which is considered to be very important for safety. The absorption peak for ice at 1.45 μm is shifted from where the peak for liquid H_2O is located and it may be possible to distinguish ice reflection from metal or water surface by processing the reflectance data [96]. Multivariate calibration is an interdisciplinary field. The natural extension to the PCR and the PLS algorithm is

neural network, which may have better prediction capability, but is even less studied in a statistical sense. The application of a MSXC laser provides a testing ground for these algorithms.

In trace gas detection, a SXC laser has some advantages over a DFB laser in developing a system for detection of new species. A SXC laser is cheap to make and can cover more spectral region than a DFB laser, whose wavelength may not be close enough to a absorption line. One critical feature which has not been achieved is to find a cheap, reliable and compact way to tell which mode the SXC laser is on and its wavelength. This may be a challenging project.

Determination of concentration, as employed in the trace gas detection by WM technique, relies on measurement of a small absorption signal on top of a large transmitted beam. In addition to the requirement for a large dynamic range of electronics, the shot noise of detectors will ultimately limit the sensitivity of detection. Photoacoustic detection is more sensitive because the signal is from only the absorbed energy and is believed to be a good alternative to measurement of transmission if the concentration is a only concern. A microphone is cheaper than a photodetector, especially for a long wavelength (> 1.7 μm) photodetector.

Developing a prototype instrument based the techniques described in this thesis for commercialization in industrial process control, environment pollution monitoring and

described in this thesis have potential to fill a niche in diode laser based trace species instrumentation. A successful attempt will need to improve the techniques to be more user-friendly and to have a good understanding of the need from potential users.

Appendix A

$$(1+x)^{1/2}=1+\frac{1}{2}x+\sum_{n=1}^{\infty}\frac{1\cdot3\cdot5\cdots(2n-1)}{2^{n+1}(n+1)!}(-1)^n x^{n+1}$$

$$\sin^{2n-1}x=\frac{(-1)^{n-1}}{2^{2n-2}}\sum_{p=0}^{n-1}\frac{(2n-1)!(-1)^p}{(2n-p-1)!p!}\sin(2n-2p-1)x$$

$$\sin^{2n}x=\frac{(-1)^n}{2^{2n-1}}\sum_{p=0}^{n-1}\frac{(2n)!(-1)^p}{(2n-p)!p!}\cos(2n-2p)x+\frac{(2n)!}{2^{2n}n!n!}$$

The a_k terms up to the order of M^6 in Eq. 17 are list below:

$$a_0=1-\frac{M^2}{16}-\frac{15M^4}{1024}+\frac{105M^6}{16384}$$

$$a_1=-i\left(\frac{M}{4}+\frac{3M^3}{128}+\frac{35M^5}{4096}\right)e^{i\psi} \qquad a_{-1}=i\left(\frac{M}{4}+\frac{3M^3}{128}+\frac{35M^5}{4096}\right)e^{-i\psi}$$

$$a_2=\left(\frac{M^2}{32}+\frac{5M^4}{512}+\frac{315M^6}{65536}\right)e^{i2\psi} \qquad a_{-2}=\left(\frac{M^2}{32}+\frac{5M^4}{512}+\frac{315M^6}{65536}\right)e^{-i2\psi}$$

$$a_3=i\left(\frac{M^3}{128}+\frac{35M^5}{8192}\right)e^{i3\psi} \qquad a_{-3}=-i\left(\frac{M^3}{128}+\frac{35M^5}{8192}\right)e^{-i3\psi}$$

$$a_4=-\left(\frac{5M^4}{2048}+\frac{63M^6}{32768}\right)e^{i4\psi} \qquad a_{-4}=-\left(\frac{5M^4}{2048}+\frac{63M^6}{32768}\right)e^{-i4\psi}$$

$$a_5=-i\frac{7M^5}{8192}e^{i5\psi} \qquad a_{-5}=i\frac{7M^5}{8192}e^{-i5\psi}$$

$$a_6=\frac{21M^6}{65536}e^{i6\psi} \qquad a^{-6}=\frac{21M^6}{65536}e^{-i6\psi}$$

Appendix B

I: *PCR algorithm (for N factors)*

Calibration:

1) Mean centre absorbance matrix $\mathbf{X}_0$ and concentration matrix $\mathbf{Y}_0$.

2) For each factor, take $\mathbf{t}_a$ = the column in $\mathbf{X}_{a-1}$ that has the highest remaining sum of squares.

3) $\mathbf{p}'_a = \mathbf{t}'_a\mathbf{X}_{a-1}/\mathbf{t}'_a\mathbf{t}_a$,

4) $\mathbf{p}'_a = \mathbf{p}'_a/\|\mathbf{p}'_a\|$ (normalization),

5) $\mathbf{t}_a = \mathbf{X}_{a-1}\mathbf{p}_a/\mathbf{p}'_a\mathbf{p}_a$,

6) $\mathbf{q}'_a = \mathbf{t}'_a\mathbf{Y}_{a-1}/\mathbf{t}'_a\mathbf{t}_a$.

Check convergence:

7) compare the $|\mathbf{t}_a|$ in step 5) with the one from the preceding iteration, if their different is smaller than a pre-specified constant, e.g., 0.001, go to step 8). If not, go to step 3).

Calculation of the residuals:

8) $\mathbf{X}_a = \mathbf{X}_{a-1} - \mathbf{t}_a\mathbf{p}'_a$,

$\mathbf{Y}_a = \mathbf{Y}_{a-1} - \mathbf{t}_a\mathbf{q}'_a$,

increase a by 1, repeat step 2) to 8) for next factor until N factors are calculated.

Prediction:

1) Mean centre input absorbance matrix **x**:

$\mathbf{x}_0' = \mathbf{x}' - \overline{\mathbf{X}}'$,

where $\overline{\mathbf{X}}$ is the centre for the calibration objects. For each factor a=1, ..., N perform steps 2) to 4).

2) Find $\mathbf{t}_a$ according by

$\mathbf{t}_a = \mathbf{x}'_{a-1}\mathbf{p}_a$.

3) Compute new residual $\mathbf{x}_a = \mathbf{x}_{a-1} - \mathbf{t}_a\mathbf{p}_a'$.

If a < N, increase a by 1 and go to 2). If a = N, go to 4).

4) Predict y by

$y = \overline{Y} + \Sigma \mathbf{t}_a\mathbf{q}_a$, sum from a = 1 to N, $\overline{Y}$ is the centre for the calibration objects.

II: *PLS algorithm (for N factors)*

Calibration:

1) Mean centre absorbance matrix $\mathbf{X}_0$ and concentration matrix $\mathbf{Y}_0$.

2) For each factor, take $\mathbf{u}_a$ = one column of $\mathbf{Y}_{a-1}$.

In the X block:

3) $\mathbf{w}'_a = \mathbf{u}'_a\mathbf{X}_{a-1}/\mathbf{u}'_a\mathbf{u}_a$,

4) $\mathbf{w}'_a = \mathbf{w}'_a/\|\mathbf{w}'_a\|$ (normalization),

5) $\mathbf{t}_a = \mathbf{X}_{a-1}\mathbf{w}_a/\mathbf{w}'_a\mathbf{w}_a$.

In Y block:

6) $\mathbf{q}'_a = \mathbf{t}'_a\mathbf{Y}_{a-1}/\mathbf{t}'_a\mathbf{t}_a$,

7) $\mathbf{q}'_a = \mathbf{q}'_a/\|\mathbf{q}'_a\|$ (normalization),

8) $\mathbf{u}_a = \mathbf{Y}_{a-1}\mathbf{q}_a/\mathbf{q}'_a\mathbf{q}_a$,

Check convergence:

9) compare the $|\mathbf{t}_a|$ in step 5) with the one from the preceding iteration, if their different is smaller than a pre-specified constant, e.g., 0.001, go to step 10). If not, go to step 3).

10) $\mathbf{p}'_a = \mathbf{t}'_a\mathbf{X}_{a-1}/\mathbf{t}'_a\mathbf{t}_a$,

11) $\mathbf{t}_a = \mathbf{t}_a\|\mathbf{p}'_a\|$,

12) $\mathbf{w}'_a = \mathbf{w}'_a\|\mathbf{p}'_a\|$,

13) $\mathbf{p}'_a = \mathbf{p}'_a/\|\mathbf{p}'_a\|$ (normalization),

14) $b_a = \mathbf{u}'_a\mathbf{t}_a/\mathbf{t}'_a\mathbf{t}_a$.

Calculation of the residuals:

15) $\mathbf{X}_a = \mathbf{X}_{a-1} - \mathbf{t}_a\mathbf{p}'_a$,

$\mathbf{Y}_a = \mathbf{Y}_{a-1} - \mathbf{t}_a\mathbf{q}'_a$,

increase a by 1, repeat step 2) to 15) for next factor until N factors are calculated.

Prediction:

1) Mean centre input absorbance matrix x:

$\mathbf{x}_o' = \mathbf{x}' - \overline{\mathbf{X}}'$,

where $\overline{\mathbf{X}}$ is the centre for the calibration objects. For each factor a=1, ..., N perform steps 2) to 4).

2) Find $\mathbf{t}_a$ according by

$\mathbf{t}_a = \mathbf{x}'_{a-1}\mathbf{w}_a$.

3) Compute new residual $\mathbf{x}_a = \mathbf{x}_{a-1} - \mathbf{t}_a\mathbf{p}_a'$. If a < N, increase a by 1 and go to 2). If

a = N, go to 4).

4) Predict y by

$y=\overline{Y}+\Sigma t_a q_a/b_a$, sum from a = 1 to N, $\overline{Y}$ is the centre for the calibration objects.

References:

1. R.N. Hall, G.E. Fenner, J.D. Kingsley, T.J. Soltys, and R.O. Carlson, "Coherent light emission from GaAs junctions," Phys. Rev. Lett. **9** 366-368(1962).

2. M.H. Anderson, J.R. Ensher, M.R. Mathews, C.E. Wieman and E.A. Cornell, "Observation of Bose-Einstein condensation in a dilute atomic vapor," Science, **269**, 198(1995).

3. R.W. Fox, C.S. Weimer, L. Hollberg and G.C. Turk, "The diode laser as a spectroscopic tool," Spectrochimica Acta Rev. **15**, 291-299(1993).

4. C.E. Wieman and L. Hollberg, "Using diode lasers for atomic physics," Rev. Sci. Instrum. **62**, 1-20(1991).

5. H.R. Telle, "Stabilization and modulation schemes of laser diodes for applied spectroscopy," Spectrochimica Acta Rev. Vol. 15, No. 5, 301-327(1993).

6. M. Fehér and P.A. Martin, "Tunable diode laser monitoring of atmospheric trace gas constituents," Spectrochimica Acta Part 1, **51**, 1579-1599(1995).

7. R.U. Martinelli, R.J. Menna, D.E. Cooper, C.B. Carlisle and H. Riris, "Near-Infrared InGaAs/InP Distributed-Feedback Lasers for Spectroscopic Applications," SPIE **2148**, 292-307(1994).

8. K. Niemax, H.Groll and C.S-Patschan, "Element analysis by diode laser spectroscopy," Spectrochimica Acta Rev. **15**, 349-377(1993).

9. P.S. Lee, R.F. Majkowski and T. A. Perry, "Tunable diode laser spectroscopy for isotope analysis—Detection of isotopic carbon monoxide in exhaled breath," IEEE Transactions on Biomedical Engineering, **38**, 966-972(1991).

10. H.C. Casey and M.B. Panish, *Heterostructure Lasers*, Academic Press: Orlando(1978).

11. B.F. Ventrudo, Ph.D. thesis, McMaster University(1993).

12. J. Buus, *Single Frequency Semiconductor Lasers*, SPIE Optical Engineering Press: Bellingham(1991).

13. P. Zorabedian, *Tunable External-Cavity Semiconductor Lasers* in Tunable lasers handbook, edited by F.J. Duarte, Academic Press, San Diego(1995).

14. J.C. Camparo, "The diode laser in atomic physics," Contemp. Phys., **26**, 443-477(1985).

enhanced single-mode tuning of InGaAsP and AlGaAs semiconductor diode lasers," Rev. Sci. Instrum. **62**, 2385-2388(1991).

16. S.Forouhar, S Keo, A. Larsson, A. Ksendzov and H. Temkin, "Low threshold continuous operation of InGaAs/InGaAsP quantum well lasers at ~2.0μm," Electron. Lett., **29**, 574-576(1993).

17. L.S. Rothman, R.R. Gamache, A. Goldman, L.R. Brown, R.A. Toth, H.M. Pickett, R.L. Poynter, J.-M. Flaud, C. Camy-Peyret, A. Barbe, N. Husson, C.P. Rinsland and M.A.H. Smith, "The HITRAN database: 1986 edition," Appl. Opt. **26**, 4058-4 4097(1987).

18. G.C. Bjorkland, "Frequency-Modulation Spectroscopy: A New Method for Measuring Weak Absorptions and Dispersions," Opt. Lett., **5**, 15-17(1980).

19. J. Reid and D. Labrie, "Second-Harmonic Detection with Tunable Diode Lasers-Comparison of Experiment and Theory," Appl. Phys. **B26**, 203-210(1981).

20. D.E. Jennings, "Absolute line strengths in ν_4, $^{12}CH_4$: a dual-beam diode laser spectrometer with sweep integration," Appl. Opt. **19**, 2695-2700(1980).

21. D.T. Cassidy and J. Reid, "Harmonic detection with tunable diode lasers: two-tone modulation," Appl.Phys. **B29**, 279(1982).

22. J.A. Silver, "Frequency-modulation spectroscopy for trace species detection: theory and comparison among experimental methods," Appl. Opt. **31**, 707-717 (1992).

23. D.E. Cooper and R.E. Warren, "Two-tone heterodyne spectroscopy with diode lasers: theory of line shapes and experimental results," J.Opt.Soc.Am. **B4**, 470-480(1987).

24. J. Faist, F. Capasso, C.Sirtori, D.L. Sivco, J.N. Baillargeon, A.L. Hutchinson, S.N.G. Chu and A.Y. Cho, "High power mid-infrared quantum cascade lasers operating above room temperature," Appl. Phys. Lett., **68**, p3680-3682(1996).

25. J.I. Malin, C.L. Felix, J.R. Meyer, C.A. Hoffman, J.F. Pinto, C.-H. Lin, P.C. Chang, S.J. Murry and S.S. Pei, "Type-II mid-IR lasers operating above room temperature," Ellectron. Lett., **32**, p1593-1594(1996).

26. C.B. Carlisle, D.E. Cooper, and H. Prier, "Quantum noise-limited FM spectroscopy with a lead-salt diode laser," Appl. Opt. **28**, 2567-2576(1989).

27. P. Werle, F. Slemr, M. Gehrts, and C. Bräuchle, "Quantum-limited FM-spectroscopy with a lead-salt diode laser," Appl. Phys. **B49**, 99-108(1989).

28. D.S. Bomse, A.C. Stanton, and J.A. Silver, "Frequency modulation and wavelength modulation spectroscopies: comparison of experimental methods using a lead-salt diode laser," Appl. Opt. **31**, 718-731(1992).

29. T.J. Johnson, F.G. Wienhold, J.P. Burrows, and G.W. Harris, "Frequency modulation spectroscopy at 1.3μm using InGaAsP lasers: a prototype field instrument for atmospheric chemistry research," Appl. Opt. **30**, 407-413(1991).

30. L.-G. Wang, D.A. Tate, H. Riris, and T.F. Gallaher, "High-Sensitivity Frequency-Modulation Spectroscopy with a GaAlAs Diode Laser," J. Opt. Soc. Am. **B6**, 2300-2308(1989).

31. J Reid, R.L. Sinclair, W.B. Grant, R.T. Menzies, "High sensitivity detection of trace gases at atmospheric pressure using tunable diode lasers," Optical and Quantum Electronics **17**, 31-39(1985).

32. C.R. Webster, R.D. May, C.A. Trimble, R.G. Chave, and J. Kendall, "Aircraft(ER-2) laser infrared absorption spectrometer(ALIAS) for in-situ stratospheric measurements of HCl, N_2O, CH_4, NO_2, and HNO_3," Appl. Opt. **33**, 454-472(1994).

33. D.T. Cassidy and J. Reid, "Atmospheric Pressure Monitoring of Trace Gases Using Tunable Diode Laser," Appl. Opt. **21**, 1185-1190(1982).

34. B.F. Ventrudo and D.T. Cassidy, "Operating characteristics of a tunable diode laser absorption spectrometer using short-external-cavity and DFB laser diodes," Appl. Opt. **29**, 5007-5013 (1990).

35. D.M. Bruce and D.T. Cassidy, "Detection of oxygen using short external cavity GaAs semiconductor diode lasers," Appl. Opt. **29**, 1327-1332(1990).

36. N. Goldstein and S.M. Adler-Golden, "Long-atmospheric-path measurements of near-visible absorption lines of O_2 isotopes and H_2O with a prototype AlGaAs laser transceiver system," Appl. Opt. **32**, 5849-5855(1993).

37. L.G. Weyer, "Near-infrared spectroscopy of organic substances," Appl. Spectr. Rev., **21**. 1-43(1985).

38. H. Martens and M. Martens, "NIR spectroscopy-Applied Philosophy," in *Near infra-red spectroscopy*, K.I. Hildrum et al. ed., (Ellis Horwood, 1992).

39. K.I. Hildrum, T. Isaksson, T. Naes and A. Tandberg ed., *Near infra-red spectroscopy*(Ellis Horwood, 1992).

40. X. Zhu and D.T. Cassidy, "Liquid detection using InGaAsP semiconductor lasers with multiple short external cavities," Appl. Opt. **35**, 4689-4693(1996).

41. Y. Uenishi, M. Tsugai and M. Mehregany, "Hybrid-integrated laser-diode micro-external mirror fabricated by (110) silicon micromachining," Electron. Lett. **31**, 965-966(1995).

42. V. Jayaraman, M.E. Heimbuch, L.A. Coldren and S.P. DenBaars, "Widely tunable continuous-wave InGaAsP/InP sampled grating lasers," Electron. Lett. **30**, 1492-1495(1994).

43. X. Zhu and D.T. Cassidy, "Liquid detection by diode lasers with multiple short external cavities," **CLEO'96** (conference on lasers and electro-optics), Anaheim, CA., June 2-7, 1996.

44. X. Zhu and D.T. Cassidy, "Liquid mixture detection by InGaAsP semiconductor lasers," **Optoelectronics'97**, SPIE, San Jose, CA., 8-14 Feb., 1997.

45. X. Zhu and D.T. Cassidy, "Electronic subtracter for trace-gas detection with InGaAsP diode lasers," Appl. Opt. **34**, 8303-8308(1995).

46. X. Zhu and D.T. Cassidy, "Modulation spectroscopy of semiconductor diode lasers by direct current modulation," submitted to Journall of Optical Society of America B, September, 1996.

47. X. Zhu and D.T. Cassidy, "Liquid mixture detection by InGaAsP semiconductor lasers," accepted for publication in the SPIE proceeding **3000**.

48. H. Asakura, K. Hagiwara, M. Lida and K. Eda, "External cavity semiconductor laser with a Fourier grating and an aspheric lens," Appl. Opt. **32**, 2031-2038(1993).

49. K.Petermann, *Laser diode modulation and noise*, Kluwer Academic Publishers, Dordrecht(1988).

50. G.P. Agrawal and N.K. Dutta, *Long-wavelength semiconductor lasers*, Van Nostrand Reinhold, New York(1986).

51. J.H. Osmundsen and N. Gade, "Influence of optical feedback on laser frequency spectrum and threshold conditions," IEEE J.Quantum Electron. **QE-19**, 465-469(1980).

52. L.J. Bonnell and D.T. Cassidy, "Alignment tolerances of short-external-cavity InGaAsP diode lasers for use as tunable single-mode sources," Appl. Opt. **28**, 4622(1989).

53. C. Voumard, R. Salathe and H. Weber, "Resonance amplifier model describing diode lasers coupled to short external resonators," Appl. Phys. **12**, 369-378(1977).

54. L.A. Coldren, K. Furuya, B.I. Miller and J.A. Reutschler, "Etched mirror and groove-coupled GaInAsP/InP laser devices for integrated optics," IEEE J. Quantum Electron. **QE-18**, 1679-1688(1982).

55. C.H. Henry and R.F. Kazarinov, "Stabilization of single frequency operation of coupled-cavity lasers," IEEE J. Quantum Electron. **QE-20**, 733-744(1984).

56. K. Uehara and H. Tai, "Remote detection of methane with a 1.66-μm diode laser," Appl. Opt. **31**, 809-814(1992).

57. D.T. Cassidy, "Trace Gas Detection Using 1.3-μm InGaAsP Diode Laser Transmitter Modules," Appl. Opt. **27**, 610-614(1988).

58. M.P. Arroyo and R.K. Hanson, "Absorption measurements of water-vapor concentration, temperature, and line-shape parameters using a tunable InGaAsP diode laser," Appl. Opt. **32**, 6104-6116(1993).

59. W. Lenth and M. Gehrtz, "Sensitive detection of NO_2 using high-frequency heterodyne spectroscopy with a GaAlAs diode laser," Appl. Phys. Lett. **47**, 1263-1265(1985).

60. H.Sasada, "1.5-μm DFB Semiconductor Laser Spectroscopy of HCN," J. Chem. Phys. **88**, 767-777(1988).

61. E.I. Moses and C.L. Tang, "High-sensitivity laser wavelength-modulation spectroscopy," Opt. Lett. **1**, 115-117(1977).

62. P. Pokrowsky, W. Zapka, F. Chu and G.C. Bjorklund, "High frequency wavelength modulation spectroscopy with diode lasers," Opt. Commun. **44**, 175-179(1983).

63. D.E. Cooper and R.E. Warren, "Frequency modulation spectroscopy with lead-salt diode lasers: a comparison of single-tone and two-tone techniques," Appl. Opt. **26**, 3726-3732(1987).

64. M. Gehrtz and G.C. Bjorklund, "Quantum-limited laser frequency-modulation spectroscopy," J. Opt. Soc. Am. **B2**, 1510-1525(1985).

65. J.M. Supplee, E.A. Whittaker and W. Lenth, "Theoretical description of frequency modulation and wavelength modulation spectroscopy," Appl. Opt. **33**, 6294-6302(1994).

66. E.A. Whittaker, M. Gehrtz and G.C. Bjorklund, "Residual amplitude modulation in laser electro-optics phase modulation," J. Opt. Soc. Am. **B5**, 1253-1256(1988).

67. G.R. Janik, C.B. Carlisle and T.F. Gallagher, "Two-tone frequency-modulation spectroscopy," J. Opt. Soc. Am. **B3**, 1070-1074(1986).

68. N.C. Wong and J.L. Hall, "High-resolution measurement of water-vapor overtone absorption in the visible by frequency-modulation spectroscopy," J. Opt. Soc. Am. **B6**, 2300-2308(1989).

semiconductor lasers," Opt. Lett. **8**, 575-577(1983).

70. P. Kauranen and V.G. Avetisov, "Determination of absorption line parameters using two-tone frequency-modulation spectroscopy with diode lasers," Opt. Commun. **106**, 213-217(1994).

71. W. Lenth, "High frequency heterodyne spectroscopy with current-modulated diode lasers," IEEE J. Quantum Electron., **QE-20**, 1045-1050(1984).

72. A. Yariv, chapter 11 in *Optical Electronics*, Saunders College Publishing, Orlando, U.S.A.(1991).

73. I.S. Gradshteyn and I.M. Ryzhik, *Table of Integrals, Series and Products*, p980(Academic, New York, 1965).

74. R.N. Hager, Jr. and R.C. Anderson, "Theory of the derivative spectrometer," J. Opt. Soc. Am. **60**, 1444-1449(1970).

75. G.N. Watson, *A Treatise on the Theory of Bessel Functions*, p151(Cambridge U. Press, Cambridge, 1966).

76. P.C.D. Hobbs, in Laser Noise, R. Roy, ed., "Shot noise limited optical measurement at baseband with noise lasers," Proc. Soc. Photo-Opt. Instrm. Eng. **1376**, 216-221(1990).

77. *The atlas of near infrared spectra*, Sadtler Research Laboratories, Philadelphia, 1981.

78. P. Geladi and B.R. Kowalski, "Partial least-squares regression: A tutorial," Analytica Chimica Acta, **185**, 1-17(1986).

79. D.M. Haaland and E.V. Thomas, "Partial Least-squares Methods for Spectral Analyses," Anal. Chem. 1988, **60**, 1193-1217.

80. J.A. Cornell, *Experiments with mixtures*, Wiley & Sons, Chichester, U.K., 1990.

81. E. Keryszig, *Advanced engineering mathematics*, Wiley & Sons Ltd, Chichester, U.K., 1988.

82. H. Ghung, M.A. Arnold, M. Rhiel and D.W. Murhammer, "Simultaneous measurements of glucose, glutamine, ammonia, lactate, and glutamate in aqueous solutions by near-infrared spectroscopy," Appl. Spectrosc. **50**, 270(1996).

83. A.R. Adams, "Band structure engineering for low-threshold high efficiency semiconductor lasers," Electron. Lett. **22**, 249-250(1986).

84. E.P. O'Reilly and A.R. Adams, "Band-structure engineering in strained semiconductor lasers," IEEE J.Quantum Electron., **30**, 366-379(1994).

85. ©Crosslight Software Inc. and National Research Council of Canada.

86. A. Verhoef, S.J. Allen, H.A.R. De Bruin, C.M.J. Jacobs and B. Heusinkveld, "Fluxes of carbon dioxide and water vapour from a Sahelian savanna," Agric. For. Meteorol., **80**, 231-248(1996).

87. J.D. Evans, T.Makino, N. Puetz, J.G. Simmons and D.A. Thompson, "Strain-induced performance improvements in long-wavelength, multiple-quantum-well ridge-waveguide lasers with all quaternary active regions," IEEE Photon. Technol. Lett., **4**, 299-301(1992).

88. B.J. Robinson, private communication, July, 1996.

89. M. Davies, private communication, September, 1996.

90. B. Lakshmi, private communication, September, 1996.

91. M. Davies, M. Dion, D.C. Houghton, J.Z. Sedivy and C.M. Vigneron, "Long-wavelength high-efficiency low-threshold InGaAsP/InP MQW lasers with compressive strain," Electron. Lett., **28**, 2004-205(1992).

92. Q.C. Zhao, private communication, October, 1996.

93. D.T. Cassidy, "Analytic Description of a Homogeneously Broadened Injection Laser," IEEE J. Quantum Electron., **QE-20**, 913-918(1984).

94. V.G. Avetisov and P. Kauranen, "Two-tone frequency-modulation spectroscopy for quantitative measurements of gaseous species: theoretical, numerical, and experimental investigation of line shapes," Appl. Opt. **35**, 4705-4723(1996).

95. J.J. Huang, C.C. Yang and D.W. Huang, "Carrier capture competition between two different quantum wells in dual-wavelength semiconductor lasers," IEEE Photon. Techn. Lett. **8**, 752-754(1996).

96. L. Kou, D. Labrie and P. Chylek, "Refractive indices of water and ice in the 0.65- to 2.5-μm spectral range," Appl. Opt. **32**, 3531-3540(1993).

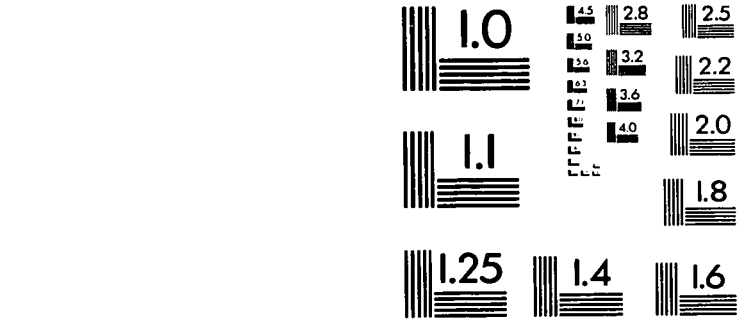

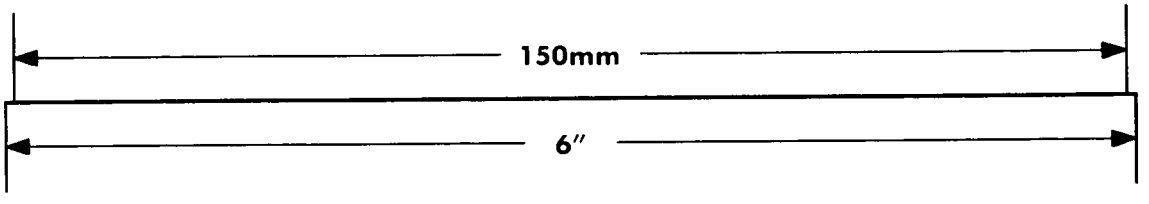

APPLIED IMAGE, Inc
1653 East Main Street
Rochester, NY 14609 USA
Phone: 716/482-0300
Fax: 716/288-5989